3. Nakamura M, Takeshita A, Nose Y. Clinical characteristics associated with myocardial infarction, arrhythmias, and sudden death in patients with vasospastic angina. *Circulation* 1987; 75:1110–1116.
4. Furberg CD, Psaty BM, Meyer JV. Nifedipine: dose-related increase in mortality in patients with coronary heart disease. *Circulation* 1995;92:1326–1331.
5. Landmesser U, Hornig B, Drexler H. Endothelial function: a critical determinant in atherosclerosis? *Circulation* 2004;109(Suppl.2):II-27–II-33.
6. Sakai K, Hirooka Y, Matsuo I, Eshima K, Shigematsu H, Shimokawa H, Takeshita A. Overexpression of eNOS in NTS causes hypotension and bradycardia in vivo. *Hypertension* 2000;36:1023–1028.
7. Kishi T, Hirooka Y, Ito K, Sakai K, Shimokawa H, Takeshita A. Cardiovascular effects of overexpression of endothelial nitric oxide synthase in the rostral ventrolateral medulla in stroke-prone spontaneously hypertensive rats. *Hypertension* 2002;39:264–268.
8. Oizumi K, Nishino H, Koike H. Antihypertensive effects of CS-905, a novel dihydropyridine calcium channel blocker in conscious hypertensive dogs. *Jpn J Pharmacol* 1990;53:264–266.
9. Oizumi K, Nishino H, Miyake S, Shiga H, Sada T, Miyamoto M, Koike H. Hemodynamic changes following long-term administration of CS-905, a novel dihydropyridine calcium channel blocker, in conscious SHR. *Jpn J Pharmacol.* 1990;54:1–6.
10. Oizumi K, Nishino H, Koike H, Sada T, Miyamoto M, Kimura T. Antihypertensive effects of CS-905, a novel dihydropyridine Ca^{++} channel blocker. *Jpn J Pharmacol* 1989;51:57–64.
11. Kuramoto K, Ichikawa S, Hirai A, Kanada S, Nakachi T, Ogihara T. Azelnidipine and amlodipine: a comparison of their pharmacokinetics and effects on ambulatory blood pressure. *Hypertens Res.* 2003;26:201–208.
12. Arita M, Hashizume T, Tanigawa K, Yamamoto H, Nishio I. A new Ca-antagonist, azelnidipine, reduced blood pressure during exercise without augmentation of sympathetic nervous system in essential hypertension: a randomized, double-blind, placebo-controlled trial. *J Cardiovasc Pharmacol* 1999;33:186–192.
13. Kobayashi N, Kobayashi K, Hara K, Higashi T, Yanaka H, Yagi S, Matsuoka H. Benidipine stimulates nitric oxide synthase and improves coronary circulation in hypertensive rats. *Am J Hypertens* 1999;12:483–491.
14. Tabrizchi R. Amlodipine and endothelial nitric oxide synthase activity. *Cardiovasc Res* 2003;59:807–809.
15. Berkels R, Taubert D, Bartels H, Breitenbach TB. Amlodipine increases endothelial nitric oxide by dual mechanisms. *Pharmacology* 2004;70:39–45.
16. Lenasi H, Kohlstedt K, Fichtlscherer B, Mülsch A, Busse R, Fleming I. Amlodipine activates the endothelial nitric oxide synthase by altering phosphorylation on Ser^{1177} and Thr^{495}. *Cardiovasc Res* 2003;59:844–853.
17. Toda N, Okamura T. The pharmacology of nitric oxide in the peripheral nervous system of blood vessels. *Pharmacol Rev* 2003;55:271–324.
18. Huang BS, Leenen FHH. Sympathoinhibitory effects of central nifedipine in spontaneously hypertensive rats on high versus regular sodium intake. *Hypertension* 1999;33:32–35.
19. Huang BS, Murzenok PP, Leenen FHH. Sympathoinhibitory and depressor responses to long-term infusion of nifedipine in spontaneously hypertensive rats. *J Cardiovasc Pharmacol* 2000;36:704–710.
20. Murzenok PP, Huang BS, Leenen FHH. Sympathoinhibition by central and peripheral infusion of nifedipine in spontaneously hypertensive rats. *Hypertension* 2000;35:631–636.
21. Huang BS, Leenen FHH. Sympathoinhibitory and depressor effects of amlodipine in spontaneously hypertensive rats. *J Cardiovasc Pharmacol* 2003;42:153–160.
22. Soong TW, Stea A, Hodson CD, Dubel SJ, Vincent SR, Snutch TP. Structure and functional expression of a member of the low voltage-activated calcium channel family. *Science* 1993;260:1133–1136.
23. Miller, RJ. Multiple calcium channels and neuronal function. *Science* 1987;235:46–52.

24. Higuchi S, Takeshita A, Ito N, Imaizumi T, Matsuguchi H, Nakamura M. Arterial pressure and heart rate responses to calcium channel blockers administered in the brain stem in rats. *Circ Res* 1985;57:244–251.
25. Kishi T, Hirooka Y, Mukai Y, Shimokawa H, Takeshita A. Atorvastatin causes depressor and sympatho-inhibitory effects with upregulation of nitric oxide synthases in stroke-prone spontaneously hypertensive rats. *J Hypertens* 2003;21:379–386.
26. Binggeli C, Corti R, Sudano I, Luscher TF, Noll G. Effects of chronic calcium channel blockade on sympathetic nerve activity in hypertension. *Hypertension* 2002;39:892–896.

Stent-Based Local Delivery of Nuclear Factor-κB Decoy Attenuates In-Stent Restenosis in Hypercholesterolemic Rabbits

Kisho Ohtani, MD, PhD; Kensuke Egashira, MD, PhD; Kaku Nakano, PhD; Gang Zhao, MD; Kouta Funakoshi, MD; Yoshiko Ihara, MD; Satoshi Kimura, MD; Ryuji Tominaga, MD, PhD; Ryuichi Morishita, MD, PhD; Kenji Sunagawa, MD, PhD

Background—Nuclear factor-κB (NF-κB) plays a critical role in the vascular response to injury. However, the role of NF-κB in the mechanism of in-stent restenosis remains unclear. We therefore tested the hypothesis that blockade of NF-κB by stent-based delivery of a cis-element "decoy" of NF-κB reduces in-stent neointimal formation.

Methods and Results—Stents were coated with a polymer containing or not containing NF-κB decoy, which represented a fast-release formulation (<7 days). Bare, polymer-coated, and NF-κB decoy–eluting stents were implanted in iliac arteries of hypercholesterolemic rabbits. Increased NF-κB activity was noted at early stages after stenting, which was suppressed by stent-based delivery of NF-κB decoy. NF-κB decoy–eluting stents also reduced monocyte infiltration and monocyte chemoattractant protein-1 expression and suppressed CD14 activation on circulating leukocytes. Importantly, NF-κB decoy–eluting stents attenuated neointimal formation on day 28. There was no evidence of an incomplete healing process (persistent inflammation, hemorrhage, fibrin deposition, impaired endothelial regeneration) at the site of NF-κB decoy–eluting stents. Transfection of NF-κB decoy suppressed proliferation of human coronary artery smooth muscle cells in vitro. No systemic adverse effects of NF-κB decoy were detected.

Conclusions—Stent-based local delivery of NF-κB decoy reduced in-stent neointimal formation with no evidence of incomplete healing. These data suggest that this strategy may be a practical and promising means for prevention of in-stent restenosis in humans. (***Circulation.*** **2006;114:2773-2779.)**

Key Words: inflammation ■ monocytes ■ restenosis ■ myocytes, smooth muscle

Each year, >1.5 million patients worldwide undergo percutaneous coronary intervention for atherothrombotic lesions. Local drug delivery by drug-eluting stents is now becoming a useful strategy for prevention of restenosis because of promising results in animal studies and clinical trials.[1,2] Currently marketed first-generation drug-eluting stents use antiproliferative drugs including rapamycin, its analogues, or paclitaxel. The current antiproliferative strategies are no longer a panacea, however, because this strategy involves potential problems such as impaired endothelial regeneration and an incomplete healing process (excessive inflammation and fibrin deposition) associated with increased risk of stent thrombosis.[3–5] Lack of long-term effects of sirolimus-eluting stents due to delayed inflammation and proliferation has been reported in a porcine coronary model.[6]

Clinical Perspective p 2779

Recent experimental and clinical studies suggest that inhibition of stent-associated inflammation (monocyte recruitment and activation) can be a promising next-generation approach.[7–9] Nuclear factor-κB (NF-κB) is a redox-sensitive transcription factor that regulates inflammation and thus plays a critical role in the vascular response to injury.[10] Activated NF-κB is detected in human atherosclerotic and restenotic lesions of smooth muscle cells, monocytes, and endothelial cells.[11] In contrast, activated NF-κB is rarely detected in normal uninjured arteries. After vascular injury, rapid activation of NF-κB in smooth muscle cells correlates with proliferation of smooth muscle cells and induced expression of NF-κB–dependent genes.[12] Recently, blockade of NF-κB by transfection of adenoviral inhibitor-κB or NF-κB "decoy" oligodeoxynucleotides attenuated restenotic changes

Received August 11, 2005; revision received October 10, 2006; accepted October 13, 2006.

From the Departments of Cardiovascular Medicine (K.O., K.E., K.N., G.Z., Y.I., K.F., K.S.) and Surgery (S.K., R.T.), Graduate School of Medical Sciences, Kyushu University, Fukuoka, Japan; and Division of Clinical Gene Therapy, Osaka University Medical School, Osaka, Japan (R.M.).

The online-only Data Supplement, consisting of expanded Methods, tables, and a figure, is available with this article at http://circ.ahajournals.org/cgi/content/full/CIRCULATIONAHA.105.582254/DC1.

Correspondence to Kensuke Egashira, MD, PhD, Department of Cardiovascular Medicine, Graduate School of Medical Science, Kyushu University, 3-1-1, Maidashi, Higashi-ku, Fukuoka 812-8582, Japan. E-mail egashira@cardiol.med.kyushu-u.ac.jp

Circulation **is available at http://www.circulationaha.org** **DOI: 10.1161/CIRCULATIONAHA.105.582254**

(neointimal formation) after balloon injury in animal models associated with reduced NF-κB–dependent genes like monocyte chemoattractant protein-1 (MCP-1).[13,14] As a clinically feasible technique, however, these gene transfer approaches are usually hampered by prolonged arterial occlusions. It has not yet been directly determined whether blockade of NF-κB inhibits neointima formation after stenting. This is important because the mechanisms underlying neointima formation differ between balloon injury and stent-induced injury, and stenting is the most frequently performed vascular interventional technique.

We therefore created the NF-κB decoy–eluting stent using polymer technology that facilitates local delivery of the NF-κB decoy oligodeoxynucleotide during stent expansion by balloon dilatation. This decoy-eluting stent strategy is a clinically feasible approach. Although local gene delivery from a polymeric plasmid DNA-coated stent has been reported, local vascular transfer of decoy oligodeoxynucleotide by polymeric-coated stent has not been reported thus far. We herein report inhibition of in-stent neointimal formation by stent-based local transfer of NF-κB decoy in vivo.

The aims of this study were (1) to create a NF-κB decoy–eluting metallic stent by the use of water-soluble polymer; (2) to evaluate the in vivo blockade of NF-κB activation by NF-κB decoy–eluting stent implantations; and (3) to determine whether the NF-κB decoy–eluting stent attenuates stent-associated inflammation and neointimal formation in vivo.

Methods

Stent Preparation

The NF-κB decoy sequences are 5′-CCTTGAAGGGATTTCCCTCC-3′ and 3′-GGAACTTCCCTAAAGGGAGG-5′. GGGATTTCCC is the consensus sequence for the NF-κB binding site. The decoy is directed against the NF-κB binding site in the promoter region that corresponds to NF-κB–responsive genes.[15,16] The decoy works to inhibit binding of this transcription factor to the promoter region.[15,16] The NF-κB decoy oligodeoxynucleotides have been shown to bind to free NF-κB, preventing NF-κB transactivation of the cytokine genes. Because NF-κB is activated immediately after stenting, we designed the NF-κB decoy–eluting stent as an early-release formulation. The 15-mm-long stainless steel balloon-expandable stent (Kawasumi Co, Osaka, Japan) was dip-coated with multiple thin layers of polyurethane containing or not containing NF-κB decoy (500 to 600 μg per stent) under sterile conditions. Another layer of decoy-free polyurethane was applied on top of the decoy-polyurethane matrix. We selected polyurethane as a polymer matrix material for stent coating because (1) it is water soluble and therefore stably absorbs NF-κB decoy oligodeoxynucleotides and (2) metallic stents coated with polyurethane containing DNA are reported to be useful for transgene delivery to the iliac arterial wall of rabbits.[17] In addition, of a number of polymer matrix materials evaluated for stent coating, polyurethane has been shown to prevent the thrombosis and inflammation that can occur with uncoated stents and some polymers used for stent coating.[18]

The coated stent was then mounted over a 3-mm balloon catheter. Uncoated bare stent mounted over the same balloon catheter was used as a control. Before implantation, all stents were sterilized with the use of ethylene oxide.

In Vitro Kinetics

In vitro kinetics studies were performed by placing a NF-κB decoy–coated stent in Tris-EDTA buffer at 37°C. The stent was periodically removed from the buffer, and the decoy eluted into the buffer was measured by a high-performance liquid chromatography system. The incremental quantities of the decoy released from the stent were plotted against time (n=8).

Stent Implantation in Animal Models

The experiments were reviewed and approved by the Committee on Ethics on Animal Experiments, Kyushu University Faculty of Medicine, and were performed according to the US National Institutes of Health *Guide for the Care and Use of Laboratory Animals*.

Male Japanese white rabbits (KBT Oriental, Tokyo, Japan) weighing 3.0 to 3.5 kg were fed a high-cholesterol diet containing 1% cholesterol and 3% peanut oil for 2 weeks before stent implantation. Animals were anesthetized and were divided randomly into 3 groups, which underwent deployment of either an uncoated bare metal stent (n=22); decoy-free polyurethane-coated stent (n=22); or NF-κB decoy–coated stent (n=22) in the right femoral artery as described previously.[9] All animals received aspirin at 20 mg/d until euthanasia from 3 days before the stent implantation procedure. After venous blood samples were taken, animals were killed with a lethal dose of anesthesia at days 3 (n=6 each), 10 (n=8 each), and 28 (n=8 each). Stented arterial sites and contralateral unstented sites were excised for biochemical, immunohistochemical, and morphometric analyses.

Histopathological and Immunohistochemical Analysis

The stented artery segments were processed as described previously.[9] The segment was divided into 2 parts at the center of the stent. The proximal part was embedded in methyl methacrylate mixed with *n*-butyl methacrylate to allow for sectioning through metal stent struts. Serial sections were stained with elastica van Gieson and hematoxylin-eosin. Neointimal area, the area within the internal elastic lamina and external elastic lamina, and the lumen area were measured by computerized morphometry. A single observer who was blinded to the experiment protocol performed morphometry. All images were captured by an Olympus microscope equipped with a digital camera (HC-2500) and were analyzed with the use of Adobe Photoshop 6.0 and Scion Image 1.62 Software.

The injury and inflammatory scores were determined at each strut site, and mean values were calculated for each stented segment as previously described[19,20] (see Table I in the online-only Data Supplement for details).

The distal part was used for immunohistochemical analysis. After stent struts were removed gently with microforceps, the tissue was dehydrated, embedded in paraffin, and cut into 5-μm-thick slices. They were subjected to immunostaining with antibodies against rabbit monocytes/macrophages (RAM-11; Dako, Glostrup, Denmark), endothelial cells (CD31; Dako), an epitope (α-p65) on the p65 subunit of NF-κB (α-p65; Boehringer Mannheim, Roche Diagnostics, Basel, Switzerland), MCP-1 (a gift from Dr Matsukawa, Kumamoto University), or nonimmune mouse IgG (Dako). The α-p65 monoclonal antibody recognizes an epitope on the p65 subunit that is masked by bound I-κB.[11] Therefore, this antibody exclusively detects activated NF-κB. For quantification of immunohistochemical images, care was taken to select stented sites with minor injury in the neointima induced by detachment of stent strut. Because this process of selecting sections with the least injury may introduce bias, at least 5 representative images were selected, and the percentage of immunopositive cells per total cells in each image was calculated. The average of the 5 images was reported for each animal.

Electrophoretic Mobility Shift Assay

The electrophoretic mobility gel shift assay was performed on nuclear extracts prepared immediately from rabbit femoral arteries after stent implantation with the method described previously.[21] For competition studies, a 50-fold molar excess of unlabeled probe for NF-κB was added. For supershift assays, 1 μg anti-p50 or anti-p65 (Santa Cruz Biotechnology, Inc, Santa Cruz, Calif) antibodies was added and incubated for 20 minutes. Nuclear extracts of HeLa cells were used as positive control.

Real-Time Quantitative Reverse Transcription Polymerase Chain Reaction

Real-time polymerase chain reaction amplification was performed with the rabbit cDNA with the use of the ABI PRISM 7000 Sequence Detection System (Applied Biosystems, Foster City, Calif) as described previously.[22] The respective polymerase chain reaction primers and TaqMan probes were designed from GenBank databases with a software program (Applied Biosystems; Table II in the online-only Data Supplement).

Fluorescence-Activated Cell Sorting

Peripheral blood was obtained at day 10 after stent implantation (n=7 each). Flow cytometry for $CD14^+$ cells was performed with the use of R-phycoerythrin–conjugated anti-CD14 (Dako). Data were analyzed by a flow cytometer and software (Becton, Dickinson and Co, Franklin Lakes, NJ).

Blood Cholesterol Measurements

Plasma total cholesterol levels were determined with commercially available kits (Wako Pure Chemical Industries, Ltd, Osaka, Japan).

Human Coronary Artery Smooth Muscle Cell Culture

This section is available in the online-only Data Supplement.

Potential Systemic Adverse Effects or Toxicity

To examine systemic adverse effects, biochemical markers were measured before and after implantation of the NF-κB decoy–eluting stent in rabbits (n=7). Five 5-year-old male cynomolgus monkeys weighing 4.2 to 5.0 kg were purchased and fed a normal diet (n=5). Biochemical markers were measured before and after intravenous injection of NF-κB decoy at 1 mg.

Statistical Analysis

Data are expressed as mean±SD. Statistical analysis of differences between the 2 groups was performed by unpaired *t* test. Statistical analysis of differences among the 3 groups was performed with the use of ANOVA and Bonferroni multiple comparison tests. A level of $P<0.05$ was considered statistically significant.

The authors had full access to the data and take responsibility for the integrity of the data. All authors have read and agree to the manuscript as written.

Results

Eluting Stent and In Vitro Release Kinetics

Scanning electron microscopy analysis revealed that the polymer coating formed a uniform film over the outer surface of the stent (Figure 1A). After balloon expansion, stretching of the polymer with no fragmentation was observed (Figure 1A). In vitro release kinetics showed an early burst release of NF-κB decoy as designed (Figure 1B).

Early Activation of NF-κB After Stenting and Effects of NF-κB Decoy–Eluting Stents

Time course and localization of NF-κB activation were examined by immunohistochemical studies with the antibody against α-p65. This antibody recognizes the I-κB binding region on the p65 component of NF-κB.[11] In the unstented artery, no positive cells for α-p65 were noted in the media and adventitia, whereas there were some positive cells in the endothelial layer (Figure 2A). On day 3, activation of NF-κB was noted in the smooth muscle cells in the media. On day 10, activation of NF-κB decreased markedly in the media, but it was noted in neointimal cells of the luminal side. On day 28,

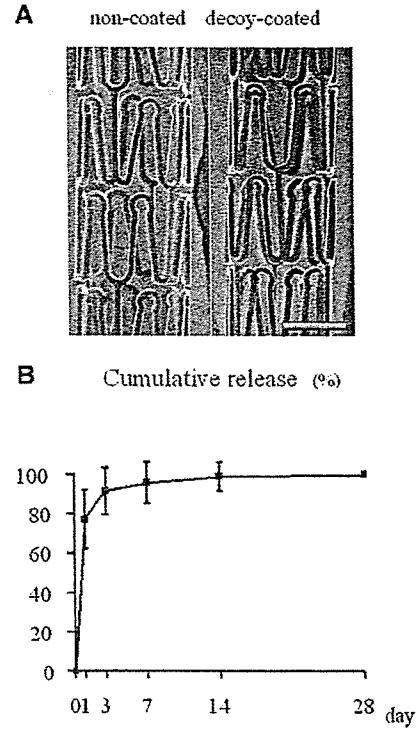

Figure 1. A, Scanning electron microscopic images of balloon-expanded uncoated stent (left) and NF-κB decoy–coated stent (right). Scale bar=1 mm. B, In vitro time course of cumulative NF-κB decoy release from the eluting stents (n=8). The percentage of incremental quantities of the decoy released from the stent was plotted against time.

NF-κB activation was rarely noted in the media and neointima, but it was noted in cells around the stent strut.

The effects of NF-κB decoy–eluting stent on NF-κB activation were examined on day 3 (Figure 2B and 2C). As expected, compared with the uncoated stent site, the number of α-p65–positive cells in the media was less ($P<0.01$) in the NF-κB decoy–eluting stent site.

To confirm immunohistochemical data, an electrophoretic mobility shift assay was performed (Figure 3). No DNA binding activity of NF-κB was noted in samples from unstented arteries. In contrast, the binding activity increased strikingly in samples from the uncoated stent site, which peaked on day 1 and gradually decreased on days 3 and 7. This NF-κB binding activity was attenuated in samples from the NF-κB–eluting stent site. Competition for increased binding of NF-κB was observed by an excess amount of NF-κB. A diminution of main band with supershifted band was observed in samples from uncoated stent sites treated with the p65 antibody but not with the p50 antibody.

Inhibitory Effects of NF-κB Decoy–Eluting Stent on Neointimal Formation

The in-stent neointima was formed equally in the uncoated stent and polyurethane-coated stent sites. Quantitative analysis demonstrated a significant reduction ($P<0.01$) of neointimal formation (neointimal area and thickness) and percent stenosis in the NF-κB decoy–eluting stent site compared with the other 2 sites (Figure 4). In contrast, there were no

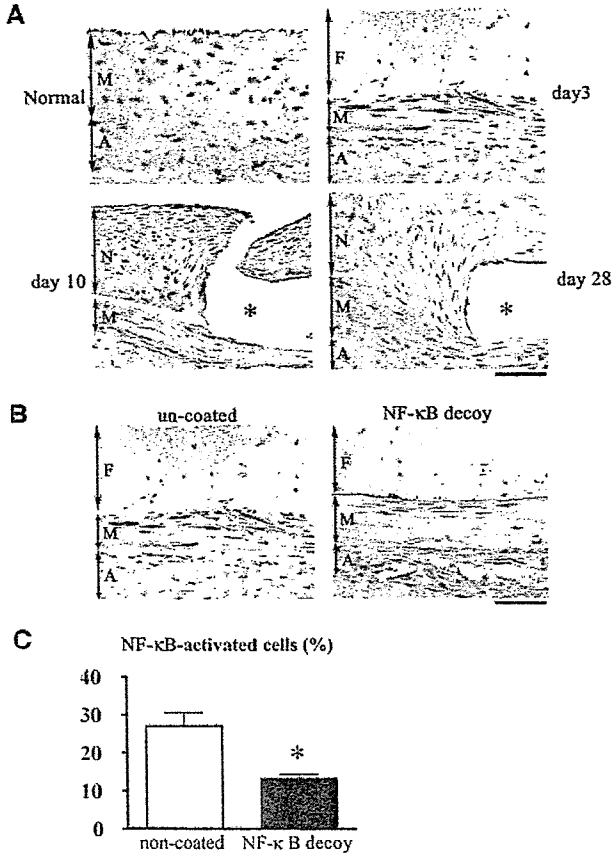

Figure 2. Immunohistochemical detection of activated NF-κB after stenting and inhibitory effects of NF-κB decoy–eluting stents on NF-κB activation. A, Immunohistochemistry of arterial cross sections stained with α-p65. *Stent strut. F indicates fibrin layer; N, neointima; M, media; and A, adventitia. Bar=50 μm. B, Artery sections from the uncoated stent site and NF-κB–eluting stent site stained immunohistochemically with the antibody against α-p65. *Stent strut. Bar=50 μm. C, Comparison of NF-κB activity between uncoated stent and NF-κB–eluting stent sites (n=6 each). Percentage of NF-κB–activated (α-p65–positive) cells is shown. *$P<0.01$ vs uncoated stents by unpaired t test.

significant differences in internal elastic lamina area, external elastic lamina area, and medial area among the 3 groups.

A semiquantitative histological scoring system demonstrated that there was no significant difference in the injury score and inflammation score among the 3 groups (Table I in the online-only Data Supplement). Endothelial cell linings, monitored by CD31 immunoreactivity, were observed equally in the 3 groups (Table I in the online-only Data Supplement). There was no significant treatment effect on serum cholesterol levels and body weight among the groups (data not shown).

Inhibitory Effects of NF-κB Decoy–Eluting Stents on Local and Systemic Inflammatory Changes

As we previously reported,[9] infiltration of RAM-11–positive macrophages around stent strut was observed at 10 days after stent implantation (Figure 5A). NF-κB decoy–eluting stents reduced such inflammatory changes (Figure 5B).

CD14 expression on circulating monocytes was examined by flow cytometry for $CD14^+$ cells as a systemic inflammation marker. Maximum fluorescence intensity of CD14 on circulating monocytes increased ($P<0.01$) 10 days after uncoated stent implantation compared with unstented controls. No increase in CD14 expression on monocytes was observed in animals implanted with NF-κB decoy–eluting stent (Figure 5C).

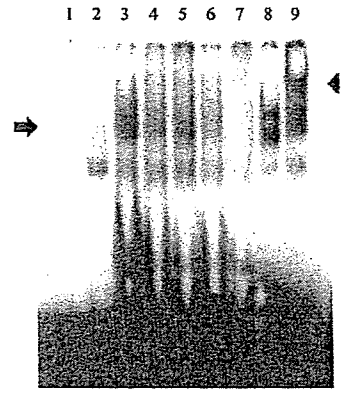

Figure 3. Assessment of activated NF-κB/DNA binding activity by electrophoretic mobility shift assay. NF-κB/DNA binding activity is determined with the use of nuclear extracts isolated from unstented and stented arteries. Lane 1, negative control (^{32}P-labeled NF-κB oligodeoxynucleotide without nuclear extract); lane 2, unstented artery; lane 3, 1-day artery after uncoated stent implantation; lane 4, 3-day artery after uncoated stent implantation; lane 5, 7-day artery after uncoated stent implantation; lane 6, 1-day artery after NF-κB decoy–eluting stent implantation; lane 7, 1-day artery after uncoated stent implantation incubated with extra amount of cold NF-κB oligodeoxynucleotide; lane 8, 1-day artery after uncoated stent implantation incubated with p50 antibody; lane 9, 1-day artery after uncoated stent implantation incubated with p65 antibody; arrowhead indicates supershift.

Inhibitory Effects of NF-κB Decoy–Eluting Stents on Expression of Proinflammatory Factors

NF-κB decoy–eluting stents reduced the increased ($P<0.01$) gene expression of MCP-1, interleukin-6, tumor necrosis factor-α, and tissue factor (Figure 6A). NF-κB decoy–eluting stents did not affect increased gene expression of interleukin-1β and vascular cell adhesion molecule-1. Immunohistochemical staining performed 10 days after stenting revealed increased immunoreactive MCP-1 in cells in the neointima and smooth muscle cells in the media, which was attenuated ($P<0.01$) in the NF-κB decoy–eluting stent group (Figure 6B).

Blockade of NF-κB Inhibits Proliferation of Human Coronary Artery Smooth Muscle Cells

The serum-induced proliferation of human coronary artery smooth muscle cells was nearly prevented ($P<0.01$) by the adenovirus-mediated gene transfer of dominant-active I-κB or by transfection of NF-κB decoy (Figure in the online-only Data Supplement).

No Adverse Systemic Effects of NF-κB Decoy

Biochemical markers were measured as described in the online-only Data Supplement. These data show that no systemic adverse effects of NF-κB decoy were noted in rabbits or monkeys.

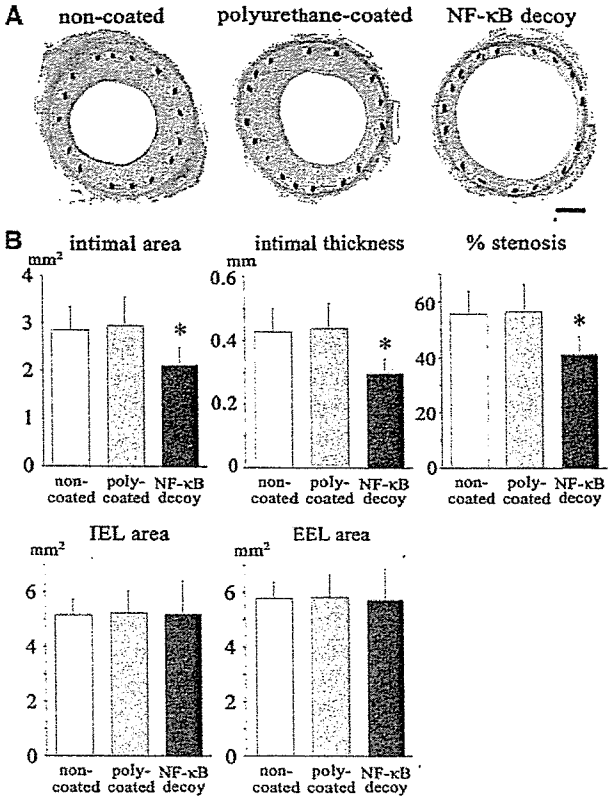

Figure 4. Inhibitory effect of NF-κB decoy–eluting stents on in-stent neointima formation. A, Iliac artery sections from the uncoated, polyurethane (poly)-coated, and NF-κB decoy–eluting stents 28 days after stenting stained with elastica van Gieson in rabbits. Bar=500 μm. B, Effect of the NF-κB decoy–eluting stents on intimal area, intimal thickness, internal elastic lamina (IEL) area, external elastic lamina (EEL) area, and percent stenosis 28 days after stenting in rabbits (n=8 each). *P<0.01 vs uncoated stents by ANOVA and Bonferroni multiple comparison tests.

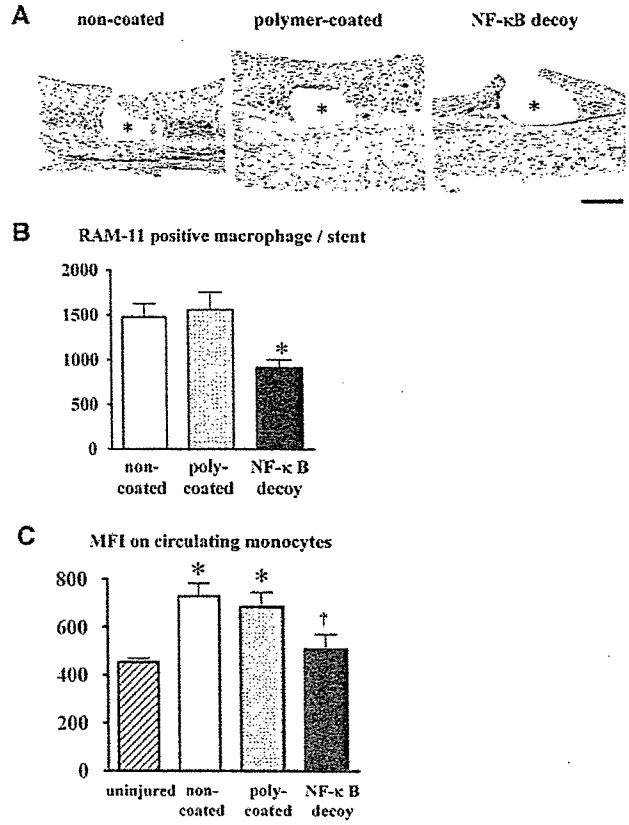

Figure 5. Effects of NF-κB decoy–eluting stents on local and systemic inflammation. A, Effect of NF-κB decoy–eluting stent on local inflammation (RAM-11–positive monocyte/macrophage) 10 days after stenting. *Stent strut. Bar=100 μm. B, Summary of quantitative analysis (n=7 each). Poly indicates polymer. *P<0.01 vs uncoated stents. C, Effects of NF-κB decoy–eluting stent on maximum fluorescence intensity (MFI) of CD14 on circulating monocytes 7 days after stenting (n=7 each). *P<0.01 vs unstented rabbits; †P<0.01 vs rabbits implanted with uncoated stents by ANOVA and Bonferroni multiple comparison tests.

Discussion

The present study reports, for the first time, the formulation of a stent-based delivery system of the NF-κB decoy oligodeoxynucleotide. A water-soluble polymer (polyurethane) was used to create a rapid-release type because NF-κB was found to be activated only at early stages but not at later stages after stenting. The present study clearly showed early activation of NF-κB after uncoated bare stenting and its inhibition by stent-based local delivery of NF-κB decoy in 2 approaches (immunostaining of a specific marker of NF-κB activation and DNA-finding assay). The inhibition of NF-κB activation was associated with reduced inflammatory changes such as reduced CD14 expression on circulating leukocytes as well as monocyte recruitment into stent sites. Although multiple factors are involved in the mechanism of decoy transfection, the mechanical force during stent expansion by the balloon dilatation procedure is likely to be a major contributing factor. The decoy might be transfected into medial and neointimal smooth muscle cells, which in turn reduced expression of various NF-κB–dependent inflammation-promoting factors. This polymeric technology-driven delivery system could be used for delivery of any other potential candidates of decoy oligodeoxynucleotides.

It has been reported that prolonged inflammatory changes were detected in arteries exposed to polymeric stent-coating materials in experimental animals[18,23] and humans.[3–5] However, no such adverse reaction was noted in this study. In addition, there was no evidence of an impaired healing process and endothelial regeneration at sites of stents coated with polyurethane alone and polyurethane plus decoy. These data suggest that the polymers used in this study may not cause an adverse reaction during a 4-week observation period.

The most important finding of the present study was inhibition of neointimal formation by stent-based delivery of NF-κB decoy. The beneficial effects of NF-κB decoy–eluting stents were associated with reduced gene expression of NF-κB–dependent genes (eg, MCP-1, interleukin-1β, interleukin-6) and with no change in NF-κB–independent genes (platelet-derived growth factor) (Figure 6). Immunoreactive MCP-1 expression was also reduced at sites of NF-κB decoy–eluting stent. These data indicate a specific function of the NF-κB decoy–eluting stent on local NF-κB activation. It is known that injury-induced inflammatory and proliferative

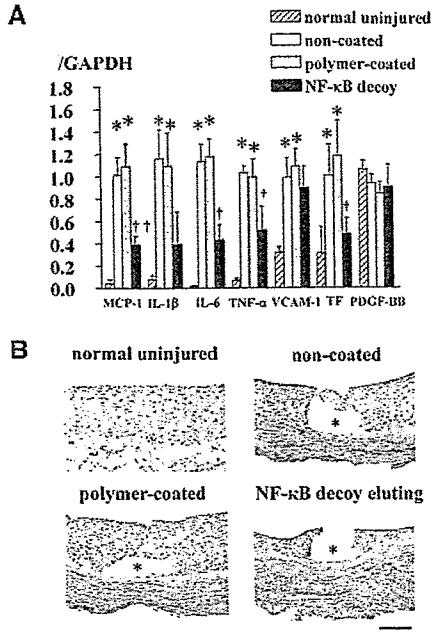

Figure 6. Effects of NF-κB decoy–eluting stents on gene expression of proinflammatory factors and immunohistochemical expression of MCP-1. A, Effect of NF-κB decoy–eluting stents on mRNA levels of various proinflammatory factors and tissue factor (TF) 10 days after stenting (n=7 to 8 each). *$P<0.01$ vs uninjured normal artery; †$P<0.05$, ††$P<0.01$ vs the control group by ANOVA and Bonferroni multiple comparison tests. B, Iliac artery sections from the uninjured normal rabbits and those from the uncoated, polyurethane-coated, and NF-κB decoy–eluting stents implanted in rabbits 10 days after stenting stained immunohistochemically with MCP-1. IL indicates interleukin; TNF, tumor necrosis factor; VCAM, vascular cell adhesion molecule; and PDGF, platelet-derived growth factor. *Stent strut. Bar=100 μm.

changes are critical in restenotic changes after vascular injury.[8,24,25] We and others have reported that (1) increased monocyte-mediated inflammation correlates positively with in-stent neointimal formation[7,26] and (2) blockade of MCP-1 reduces neointimal formation after vascular injury.[9,27,28] Because the NF-κB–eluting stent reduced inflammation and MCP-1 expression in this study, the beneficial effects of NF-κB decoy–eluting stents can be attributable at least in part to inhibition of MCP-1–related inflammation resulting from reduced NF-κB activation. Otherwise, emerging evidence suggests that NF-κB regulates proliferation of vascular smooth muscle cells.[29,30] In this regard, we found that blockade of NF-κB activation by transfection of NF-κB decoy or dominant-active I-κB suppressed proliferation of human coronary artery smooth muscle cells in vitro. Therefore, it is also likely that NF-κB decoy–eluting stents might inhibit proliferation of vascular smooth muscle cells induced by NF-κB activation.

There are several caveats in our present findings in regard to potential clinical applicability. First, application of the present findings to treatment of restenosis in humans could be limited because the ideal animal model for drug-eluting stent evaluation is uncertain according to the recommendation from the consensus group.[31] They stated that the coronary arteries in pigs and iliac-femoral arteries of rabbits are suitable in that their size, access, and injury response are similar to those of human vessels and therefore they allow examination of devices that might be used in clinical evaluation. Thus, the rabbit peripheral artery model is considered an acceptable model of choice. Second, the observed efficacy and safety of NF-κB decoy and polymer at 28 days may be too short. Third, potential adverse effects or toxicity of NF-κB decoy may be important. In histopathological analysis, no adverse reactions such as incomplete healing or impaired endothelial regeneration were noted. Measurements of serum blood markers (glucose, aspartate aminotransferase, alanine aminotransferase, creatine kinase, γ-GTP, and C-reactive protein in Tables III and IV in the online-only Data Supplement) showed no systemic adverse effects. Because the dose of NF-κB decoy (500 to 600 μg per body) coated on the stent was very low from a toxicological point of view, our decoy-coated stent may not cause any toxicity in vivo. It has been reported that repeated bolus administration of high doses (eg, 10 mg/kg every other day for 28 days in monkeys, 20 mg/kg every other day for 28 days in mice) causes kidney damage.[32] In addition, we recently completed a clinical trial to test the feasibility and safety of NF-κB decoy in which NF-κB decoy at doses of 1000, 2000, or 4000 μg per body was transfected into the stented coronary artery sites via a channel balloon catheter immediately after successful percutaneous coronary intervention in 16 patients with flow-limiting coronary stenosis. The initial 2 cases have been reported,[33] and they showed no evidence of restenosis or systemic adverse effects during the 6-month observation period. Overall, these data support the notion that this NF-κB decoy–eluting stent system can be applied to the clinical setting.

In conclusion, the present study supports the experimental evidence that stent-based local delivery of NF-κB decoy reduces in-stent neointimal formation by inhibiting NF-κB–dependent gene expression and inflammation and perhaps by inhibiting proliferation of vascular smooth muscle cells. Inhibition of stent-associated inflammation by the NF-κB decoy–eluting stent may be a promising next-generation approach for the prevention of restenosis. Further preclinical studies and clinical trials are needed to prove this hypothesis.

Sources of Funding

This study was supported by grants-in-aid for scientific research (14657172, 14207036) from the Ministry of Education, Science, and Culture, Tokyo, Japan; by health science research grants (Research on Translational Research) from the Ministry of Health, Labor, and Welfare, Tokyo, Japan; and by the Program for Promotion of Fundamental Studies in Health Sciences of the Organization for Pharmaceutical Safety and Research, Tokyo, Japan.

Disclosures

Drs Egashira and Morishita hold a patent on the results reported in the present study. The remaining authors report no conflicts.

References

1. Babapulle MN, Eisenberg MJ. Coated stents for the prevention of restenosis, part I. *Circulation.* 2002;106:2734–2740.
2. Babapulle MN, Eisenberg MJ. Coated stents for the prevention of restenosis, part II. *Circulation.* 2002;106:2859–2866.
3. Virmani R, Farb A, Guagliumi G, Kolodgie FD. Drug-eluting stents: caution and concerns for long-term outcome. *Coron Artery Dis.* 2004;15:313–318.
4. Virmani R, Guagliumi G, Farb A, Musumeci G, Grieco N, Motta T, Mihalcsik L, Tespili M, Valsecchi O, Kolodgie FD. Localized hypersensi-

tivity and late coronary thrombosis secondary to a sirolimus-eluting stent: should we be cautious? *Circulation*. 2004;109:701–705.
5. McFadden EP, Stabile E, Regar E, Cheneau E, Ong AT, Kinnaird T, Suddath WO, Weissman NJ, Torguson R, Kent KM, Pichard AD, Satler LF, Waksman R, Serruys PW. Late thrombosis in drug-eluting coronary stents after discontinuation of antiplatelet therapy. *Lancet*. 2004;364:1519–1521.
6. Carter AJ, Aggarwal M, Kopia GA, Tio F, Tsao PS, Kolata R, Yeung AC, Llanos G, Dooley J, Falotico R. Long-term effects of polymer-based, slow-release, sirolimus-eluting stents in a porcine coronary model. *Cardiovasc Res*. 2004;63:617–624.
7. Farb A, Weber DK, Kolodgie FD, Burke AP, Virmani R. Morphological predictors of restenosis after coronary stenting in humans. *Circulation*. 2002; 105:2974–2980.
8. Egashira K. Molecular mechanisms mediating inflammation in vascular disease: special reference to monocyte chemoattractant protein-1. *Hypertension*. 2003;41:834–841.
9. Ohtani K, Usui M, Nakano K, Kohjimoto Y, Kitajima S, Hirouchi Y, Li XH, Kitamoto S, Takeshita A, Egashira K. Antimonocyte chemoattractant protein-1 gene therapy reduces experimental in-stent restenosis in hypercholesterolemic rabbits and monkeys. *Gene Ther*. 2004;11:1273–1282.
10. Collins T, Cybulsky MI. NF-kappaB: pivotal mediator or innocent bystander in atherogenesis? *J Clin Invest*. 2001;107:255–264.
11. Brand K, Page S, Rogler G, Bartsch A, Brandl R, Knuechel R, Page M, Kaltschmidt C, Baeuerle PA, Neumeier D. Activated transcription factor nuclear factor-kappa B is present in the atherosclerotic lesion. *J Clin Invest*. 1996;97:1715–1722.
12. Landry DB, Couper LL, Bryant SR, Lindner V. Activation of the NF-kappa B and I kappa B system in smooth muscle cells after rat arterial injury: induction of vascular cell adhesion molecule-1 and monocyte chemoattractant protein-1. *Am J Pathol*. 1997;151:1085–1095.
13. Breuss JM, Cejna M, Bergmeister H, Kadl A, Baumgartl G, Steurer S, Xu Z, Koshelnick Y, Lipp J, De Martin R, Losert U, Lammer J, Binder BR. Activation of nuclear factor-kappa B significantly contributes to lumen loss in a rabbit iliac artery balloon angioplasty model. *Circulation*. 2002;105: 633–638.
14. Yamasaki K, Asai T, Shimizu M, Aoki M, Hashiya N, Sakonjo H, Makino H, Kaneda Y, Ogihara T, Morishita R. Inhibition of NFkappaB activation using cis-element 'decoy' of NFkappaB binding site reduces neointimal formation in porcine balloon-injured coronary artery model. *Gene Ther*. 2003;10:356–364.
15. Morishita R, Higaki J, Tomita N, Ogihara T. Application of transcription factor "decoy" strategy as means of gene therapy and study of gene expression in cardiovascular disease. *Circ Res*. 1998;82:1023–1028.
16. Kitamoto S, Egashira K, Kataoka C, Koyanagi M, Katoh M, Shimokawa H, Morishita R, Kaneda Y, Sueishi K, Takeshita A. Increased activity of nuclear factor-kappaB participates in cardiovascular remodeling induced by chronic inhibition of nitric oxide synthesis in rats. *Circulation*. 2000;102:806–812.
17. Takahashi A, Palmer-Opolski M, Smith RC, Walsh K. Transgene delivery of plasmid DNA to smooth muscle cells and macrophages from a biostable polymer-coated stent. *Gene Ther*. 2003;10:1471–1478.
18. van der Giessen WJ, Lincoff AM, Schwartz RS, van Beusekom HM, Serruys PW, Holmes DR Jr, Ellis SG, Topol EJ. Marked inflammatory sequelae to implantation of biodegradable and nonbiodegradable polymers in porcine coronary arteries. *Circulation*. 1996;94:1690–1697.
19. Schwartz RS, Huber KC, Murphy JG, Edwards WD, Camrud AR, Vlietstra RE, Holmes DR. Restenosis and the proportional neointimal response to coronary artery injury: results in a porcine model. *J Am Coll Cardiol*. 1992;19:267–274.
20. Makkar R, Whiting J, Li A, Honda H, Fishbein MC, Knapp FF, Hausleiter J, Litvack F, Eigler NL. Effects of beta(−)-emitting (188)Re balloon in stented porcine coronary arteries: an angiographic, intravascular ultrasound, and histomorphometric study. *Circulation*. 2000;102:3117–3123.
21. Ohtani K, Egashira K, Usui M, Ishibashi M, Hiasa KI, Zhao Q, Aoki M, Kaneda Y, Morishita R, Takeshita A. Inhibition of neointimal hyperplasia after balloon injury by cis-element 'decoy' of early growth response gene-1 in hypercholesterolemic rabbits. *Gene Ther*. 2004;11:126–132.
22. Ohtani K, Egashira K, Hiasa K, Zhao Q, Kitamoto S, Ishibashi M, Usui M, Inoue S, Yonemitsu Y, Sueishi K, Sata M, Shibuya M, Sunagawa K. Blockade of vascular endothelial growth factor suppresses experimental restenosis after intraluminal injury by inhibiting recruitment of monocyte lineage cells. *Circulation*. 2004;110:2444–2452.
23. Lincoff AM, Furst JG, Ellis SG, Tuch RJ, Topol EJ. Sustained local delivery of dexamethasone by a novel intravascular eluting stent to prevent restenosis in the porcine coronary injury model. *J Am Coll Cardiol*. 1997;29:808–816.
24. Egashira K. Clinical importance of endothelial function in arteriosclerosis and ischemic heart disease. *Circ J*. 2002;66:529–533.
25. Griendling KK, FitzGerald GA. Oxidative stress and cardiovascular injury, part II: animal and human studies. *Circulation*. 2003;108:2034–2040.
26. Welt FG, Rogers C. Inflammation and restenosis in the stent era. *Arterioscler Thromb Vasc Biol*. 2002;22:1769–1776.
27. Usui M, Egashira K, Ohtani K, Kataoka C, Ishibashi M, Hiasa K, Katoh M, Zhao Q, Kitamoto S, Takeshita A. Anti-monocyte chemoattractant protein-1 gene therapy inhibits restenotic changes (neointimal hyperplasia) after balloon injury in rats and monkeys. *FASEB J*. 2002;16:1838–1840.
28. Egashira K, Zhao Q, Kataoka C, Ohtani K, Usui M, Charo IF, Nishida K, Inoue S, Katoh M, Ichiki T, Takeshita A. Importance of monocyte chemoattractant protein-1 pathway in neointimal hyperplasia after periarterial injury in mice and monkeys. *Circ Res*. 2002;90:1167–1172.
29. Bellas RE, Lee JS, Sonenshein GE. Expression of a constitutive NF-kappa B-like activity is essential for proliferation of cultured bovine vascular smooth muscle cells. *J Clin Invest*. 1995;96:2521–2527.
30. Lemarie CA, Esposito B, Tedgui A, Lehoux S. Pressure-induced vascular activation of nuclear factor-kappaB: role in cell survival. *Circ Res*. 2003;93: 207–212.
31. Schwartz RS, Edelman ER, Carter A, Chronos N, Rogers C, Robinson KA, Waksman R, Weinberger J, Wilensky RL, Jensen DN, Zuckerman BD, Virmani R. Drug-eluting stents in preclinical studies: recommended evaluation from a consensus group. *Circulation*. 2002;106:1867–1873.
32. Henry SP, Bolte H, Auletta C, Kornbrust DJ. Evaluation of the toxicity of ISIS 2302, a phosphorothioate oligonucleotide, in a four-week study in cynomolgus monkeys. *Toxicology*. 1997;120:145–155.
33. Suzuki J, Ito H, Goto R, Morishita R, Egashira K, Isobe M. Initial clinical cases of the use of a NF-kappaB decoy at the site of coronary stenting for the prevention of restenosis. *Circ J*. 2004;68:270–271.

CLINICAL PERSPECTIVE

Although first-generation drug-eluting stents are effective in reducing the rate of restenosis, the drug-eluting stent has no effect on the incidence of cardiovascular events compared with the bare-metal stent. In addition, recent clinical studies have demonstrated that drug-eluting stents increase the incidence of late stent thrombosis, leading to acute myocardial infarction and death after the discontinuation of clopidogrel. These serious late thrombotic events are thought to result from impaired endothelial regeneration and an incomplete healing process because of the drugs or polymers used in the construction of drug-eluting stents. Therefore, the formulation of a novel drug-eluting stent system with fewer adverse effects is warranted. In the present study, we formulate a nuclear factor-κB (NF-κB) decoy–eluting stent with biocompatible polymer technology and report inhibition of neointimal formation by stent-based delivery of NF-κB decoy. Importantly, no histopathological evidence of impaired endothelial regeneration and healing process was noted at sites of stents coated with polymer alone and polymer plus decoy. These data support the experimental evidence that the NF-κB decoy–eluting stent is effective in reducing in-stent neointimal formation and thrombosis. Our previous clinical trial testing the feasibility and safety of NF-κB decoy supports the notion that this NF-κB decoy–eluting stent system can be applied to the clinical setting. Ultimately, we propose that this system be used to treat vulnerable plaques leading to acute coronary syndrome and stroke.

Angiotensin II Type 1 Receptor Blocker Attenuates Exacerbated Left Ventricular Remodeling and Failure in Diabetes–Associated Myocardial Infarction

Hidenori Matsusaka, MD, PhD, Shintaro Kinugawa, MD, PhD,† Tomomi Ide, MD, PhD,* Shouji Matsushima, MD,* Tetsuya Shiomi, MD, PhD,* Toru Kubota, MD, PhD,* Kenji Sunagawa, MD, PhD,* and Hiroyuki Tsutsui, MD, PhD†*

Abstract: Diabetes mellitus adversely affects the outcomes in patients with myocardial infarction (MI), due in part to the exacerbation of left ventricular (LV) remodeling. Although angiotensin II type 1 receptor blocker (ARB) has been demonstrated to be effective in the treatment of heart failure, information about the potential benefits of ARB on advanced LV failure associated with diabetes is lacking. To induce diabetes, male mice were injected intraperitoneally with streptozotocin (200 mg/kg). At 2 weeks, anterior MI was created by ligating the left coronary artery. These animals received treatment with olmesartan (0.1 mg/kg/day; n = 50) or vehicle (n = 51) for 4 weeks. Diabetes worsened the survival and exaggerated echocardiographic LV dilatation and dysfunction in MI. Treatment of diabetic MI mice with olmesartan significantly improved the survival rate (42% versus 27%, $P < 0.05$) without affecting blood glucose, arterial blood pressure, or infarct size. It also attenuated LV dysfunction in diabetic MI. Likewise, olmesartan attenuated myocyte hypertrophy, interstitial fibrosis, and the number of apoptotic cells in the noninfarcted LV from diabetic MI. Post-MI LV remodeling and failure in diabetes were ameliorated by ARB, providing further evidence that angiotensin II plays a pivotal role in the exacerbated heart failure after diabetic MI.

Key Words: myocardial infarction, diabetes mellitus, heart failure, remodeling, apoptosis

(*J Cardiovasc Pharmacol*™ 2006;48:95–102)

INTRODUCTION

Diabetes mellitus (DM) is one of the largest comorbidities of patients with acute myocardial infarction (MI). Diabetic patients who have had MI have a higher incidence of death than do nondiabetic patients, both in the acute phase and on long-term follow-up.[1] The excess mortality of diabetic patients results primarily from the development of heart failure and recurrent MI.[2] MI frequently produces progressive left ventricular (LV) dilatation associated with hypertrophy of noninfarcted LV. These changes in LV geometry, referred to as remodeling, contribute to the development of depressed cardiac function.[3] Several mechanisms, whether alone or in combination, may adversely affect LV remodeling and failure after MI in diabetic patients; such mechanisms include severe coronary artery disease, impaired vasodilatory reserve of coronary arteries, and preexisting LV dysfunction due to diabetic cardiomyopathy.[4] Clinical studies in patients with acute MI showed that the mortality is higher in diabetic patients despite similar coronary patency rates, suggesting that the exacerbation of LV dysfunction after MI in the presence of DM may play a major role.[5] In fact, our recent experimental studies demonstrated that the streptozotocin (STZ)–induced hyperglycemia exacerbated the progressive LV chamber dilatation and contractile dysfunction in a murine model of MI.[6] In diabetic MI mice, myocyte hypertrophy and apoptosis in association with interstitial fibrosis were more enhanced in diabetic post-MI hearts. We thus considered that these remodeling processes might be mutually reinforcing in the setting of MI associated with diabetes, and DM may further enhance the development of heart failure.

Angiotensin-converting enzyme (ACE) inhibitors and angiotensin II (AngII) type 1 receptor blockers (ARBs) have been shown to decrease the mortality and morbidity of patients with MI and heart failure.[7–9] Experimental evidence indicates that these drugs are effective in limiting post-MI LV remodeling and failure.[10–12] Moreover, ACE inhibitors and ARBs have been demonstrated to prevent or retard the development of diabetic complications including both microangiopathy and macroangiopathy.[13,14]

It has not yet been determined, however, whether AngII plays a key role in the exacerbation of post-MI failure in the

Received for publication June 7, 2006; accepted August 5, 2006.
From the *Department of Cardiovascular Medicine, Graduate School of Medical Sciences, Kyushu University, Fukuoka; and the †Department of Cardiovascular Medicine, Hokkaido University Graduate School of Medicine, Sapporo, Japan.
This study was supported in part by grants from the Ministry of Education, Science, and Culture (No. 12670676, 14370230, 17390223, 17659223) and SANKYO CO., LTD.
Reprints: Hiroyuki Tsutsui, MD, PhD, Department of Cardiovascular Medicine, Hokkaido University Graduate School of Medicine, Kita-15, Nishi-7, Kita-ku, Sapporo 060-8638, Japan (e-mail: htsutsui@med.hokudai.ac.jp).

presence of DM. The present study was thus performed to determine the effects of an ARB on the accelerated LV remodeling after MI associated with DM. Furthermore, various cellular and molecular mechanisms were evaluated to further elucidate critical pathways implicated in this model and in mediating cardiac protection by ARBs in diabetes-associated post-MI LV remodeling.

METHODS

Experimental Design

The study was approved by our Institutional Animal Research Committee and conformed to the animal care guidelines of the American Physiological Society.

DM was induced in male CD-1 mice (5–7 weeks old; 25-35 g body weight) by intraperitoneal injection of STZ (200 mg/kg body weight).[6] Tail vein blood glucose was measured 5 days after injection to ensure induction of diabetes. As a control, vehicle (0.1 mol/L citrate buffer, pH 4.5) was injected in another group of mice. At 2 weeks after injection, MI was created in STZ-injected mice (DM-MI group) by ligating the left coronary artery.[6] After the creation of MI, these animals were further randomized to be treated with an ARB, olmesartan (0.1 mg /kg body weight/day in osmotic minipump, SANKYO; DM-MI+Olmesartan group) or to receive vehicle (DM-MI+Vehicle group). Sham operation without ligating the coronary artery was also performed (Control groups), and these animals were also randomized to be treated with olmesartan or to receive vehicle.

All 4 groups of mice (Control+Vehicle, n = 11; Control+Olmesartan, n = 11; DM-MI+Vehicle, n = 51; DM-MI+Olmesartan, n = 50) were followed for further 4 weeks (Fig. 1).

Survival

During the study period of 6 weeks (2 weeks after vehicle or STZ injection and further 4 weeks after surgery), cages were inspected daily for deceased animals. All deceased mice were examined for the presence of pleural effusion and cardiac rupture.

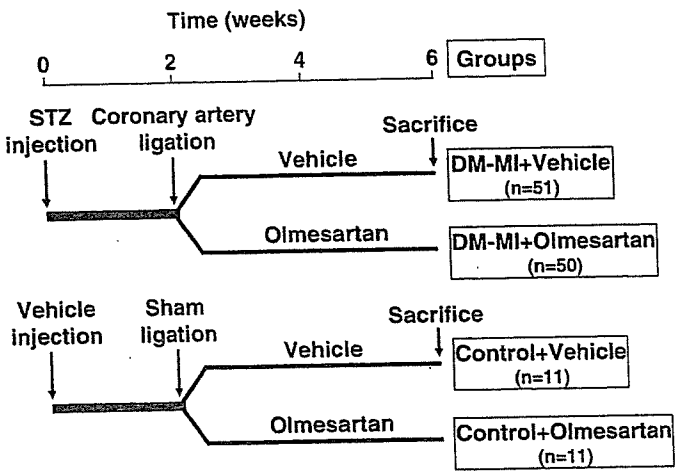

FIGURE 1. Experimental protocol. STZ, streptozotocin; DM, diabetes mellitus; MI, myocardial infarction.

Blood Glucose

Before sacrifice, venous blood samples (0.5 mL) were collected for determination of blood glucose levels.

Echocardiography and Hemodynamics

Echocardiographic studies were performed under light anesthesia with tribromoethanol/amylene hydrate (Avertin; 2.5% wt/vol, 8 μL/g intraperitoneally) and spontaneous respiration. A 2-dimensional parasternal short-axis view of the LV was obtained at the level of the papillary muscles. In general, the best views were obtained with the transducer lightly applied to the mid upper left anterior chest wall. The transducer was then gently moved cephalad or caudad and angulated until desirable images were obtained. After it was ensured that the imaging was on axis (on the basis of LV cavity roundness), two-dimensional targeted M-mode tracings were recorded at a paper speed of 50 mm/sec. Under the same anesthesia with Avertin, a 1.4 French micromanometer-tipped catheter (Millar Instruments) was inserted into the right carotid artery and then advanced into the LV to measure LV pressures.[6] One subset of investigators, who were not informed of the experimental groups, performed in vivo LV function studies.

Our validation study confirmed that the intraobserver and interobserver variabilities for our echocardiographic measurements of LV dimensions and fractional shortening were excellent, and the measurements made in the same animals on separate days were highly reproducible.[15]

Tissue Preparation and Morphometric Analysis

The heart was excised and dissected into the right and left ventricles, including the septum. The left ventricle was cut into 3 transverse sections; apex, middle ring, and base. From the middle ring, 5-μm sections were cut and stained with Masson's trichrome. The boundary lengths of the infarcted and noninfarcted endocardial and epicardial surfaces were traced with a planimeter digital image analyzer.

Infarct size (fraction of the infarcted LV) was calculated as the average of all slices and expressed as the percentage of length of circumference.[6] Myocyte cross-sectional area and collagen volume fraction were determined by quantitative morphometry of tissue sections from mid-LV.[6]

Myocardial AngII Type 1 (AT1) Receptor

The myocardial tissues with MI were carefully dissected into 3 parts: the infarcted LV, the border zone LV with the peri-infarct rim (a 1-mm rim of normal-appearing tissue), and the remaining noninfarcted (remote) LV. Total RNA was extracted from each sample by the acid guanidinium thiocyanate-phenol-chloroform method (ISOGEN, Nippon Gene).[16] Myocardial AT_1 receptor gene expression was analyzed by real-time quantitative reverse transcription–polymerase chain reaction (RT-PCR) with the use of the TaqMan system on the basis of real-time detection of accumulated fluorescence (ABI Prism 7000, Applied Biosystems) and was normalized in relation to the expression of an endogenous control, glyceraldehydes-3-phosphate-dehydrogenase (GAPDH).

Myocardial TGF-β and MMPs/TIMPs

Transforming growth factor-β (TGF-β) and matrix metalloproteinases (MMPs), including MMP-1, -2, -3, -8, and -9, as well as tissue inhibitors of MMPs (TIMPs), including TIMP-1, -2, -3, and -4, mRNA levels were determined by multiprobe ribonuclease protection assay (RPA, RiboQuant, PharMingen) according to the methods described previously.[17] Each value was normalized to that of GAPDH in each template set as an internal control, followed by calculation as a ratio to Control+Vehicle.

Apoptosis

Tissue sections from the mid-LV were stained with terminal deoxynucleotidyl transferase-mediated dUTP nick end-labeling (TUNEL) staining.[6] Staining with hematoxylin was carried out on the same section for visualization of nuclei. The number of TUNEL-positive nuclei was counted, and the data were normalized per 10^5 total nuclei identified by hematoxylin-positive staining in the same sections. The proportion of apoptotic cells was counted in the noninfarcted LV.

We further examined whether apoptosis is present in the noninfarcted LV by the more sensitive ligation-mediated PCR fragmentation assays (Maxim Biotech).

Statistical Analyses

Data are expressed as means ± SEM. Comparison of survival was performed by the Kaplan-Meier analysis. For multiple-group comparisons, ANOVA followed by Bonferroni's t test was performed. $P < 0.05$ was considered statistically significant.

RESULTS

We employed 4 groups of Control+Vehicle (n = 11), Control+Olmesartan (n = 11), DM-MI+Vehicle (n = 51), and DM-MI+Olmesartan (n = 50) mice in the present study. The survival analysis was performed in all of these mice. Subsequent echocardiographic and hemodynamic measurements were performed in the 6-week survivors; 11 Control+Vehicle, 11 Control+Olmesartan, 14 DM-MI+Vehicle, and 21 DM-MI+Olmesartan mice. These measurements could not be accomplished in 2 DM-MI+Vehicle and 9 DM-MI+Olmesartan mice due to the technical difficulties. The surviving mice were further divided into 2 groups; those for the subsequent histological analysis, including infarct size, myocyte cross-sectional area, and collagen volume fraction as well as TUNEL staining (5 Control+Vehicle, 5 Control+Olmesartan, 5 DM-MI+Vehicle, and 5 DM-MI+Olmesartan), and those for the biochemical assay including TGF-β and MMPs/TIMPs (6 Control+Vehicle, 6 Control+Olmesartan, 8 DM-MI+Vehicle, and 8 DM-MI+Olmesartan).

Survival and Blood Glucose

The mortality rates during 24 hours after ligation were 15% and 19% in DM-MI+Vehicle and DM-MI+Olmesartan mice, respectively (P = NS). Survival rates during the study period were significantly higher in DM-MI+Olmesartan than in DM-MI+Vehicle (Fig. 2). Death was suspected to be attributable to heart failure and/or arrhythmia. A single DM+MI+Vehicle (2%) and 1 DM-MI+Olmesartan (2%) mice died from LV rupture (P = NS).

Blood glucose levels at 5 days as well as 6 weeks after injection were significantly higher in the diabetic mice than in the nondiabetic mice, but they were not significantly different between DM-MI+Vehicle and DM-MI+Olmesartan mice (Table 1).

Echocardiography and Hemodynamics

In comparison with control mice, DM-MI mice showed LV dilatation and dysfunction by echocardiography, both of which were significantly ameliorated in DM-MI+Olmesartan mice (Fig. 3 and Table 1).

Heart rate was comparable among all groups (Table 1). Mean aortic blood pressure was lower in DM-MI groups than in the control groups, but there was no significant difference between DM-MI+Vehicle and DM-MI+Olmesartan. LV end-diastolic pressure (EDP) was increased in DM-MI+Vehicle mice and was significantly reduced in DM-MI+Olmesartan mice. LV dP/dt_{max} was decreased in DM+MI groups and tended to be higher in DM+MI-Olmesartan than in DM-MI+Vehicle but did not reach statistical significance (P = 0.09).

Organ Weights

Body weight was lower in DM-MI mice (Table 1), as previously observed.[6] In contrast, the tibial length was similar among all groups. Coinciding with an increased LV EDP, lung weight/tibial length was increased in the DM-MI groups, and this increase was significantly attenuated by olmesartan. The

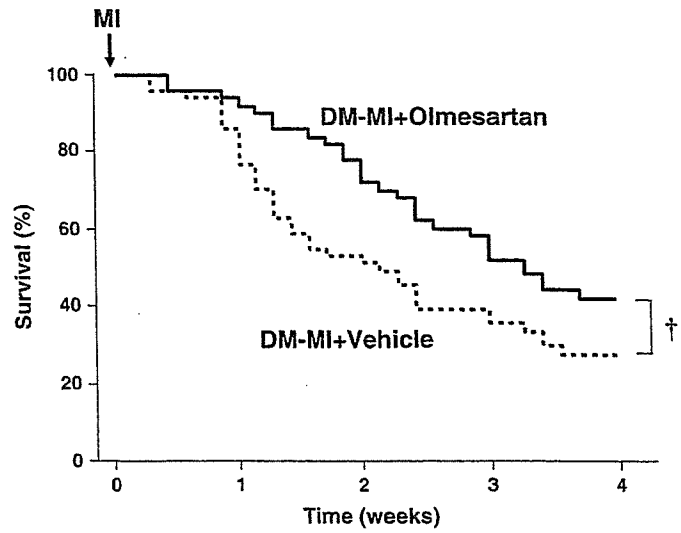

FIGURE 2. Kaplan-Meier survival analysis. Percentages of surviving DM-MI+Vehicle (n = 51) and DM-MI+Olmesartan (n = 50) mice were plotted. Overall survival was significantly higher in DM-MI+Olmesartan than in DM-MI+Vehicle. †$P <$ 0.01 for difference from the DM-MI+Vehicle group.

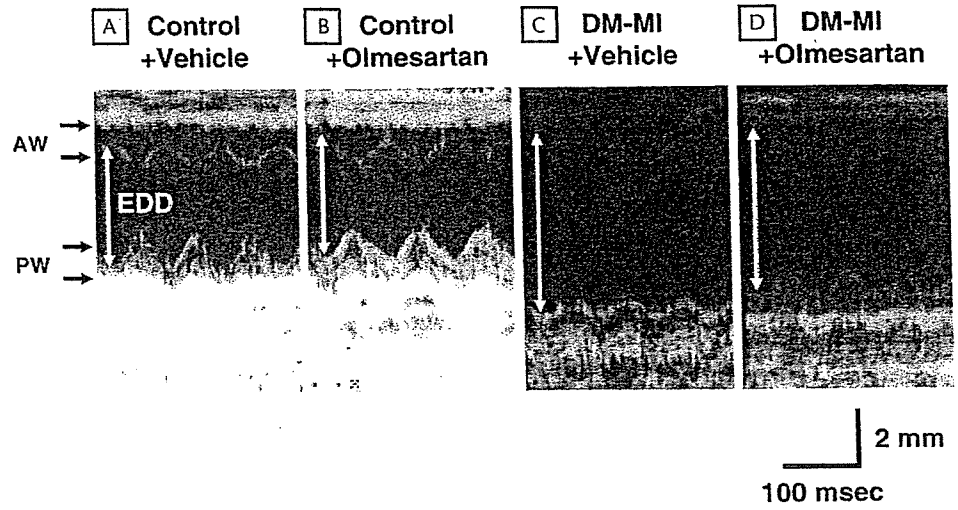

FIGURE 3. M-mode echocardiograms obtained from Control+Vehicle (A), Control+Olmesartan (B), DM-MI+Vehicle (C), and DM-MI+Olmesartan (D) 4 weeks after surgery. AW, anterior wall; PW, posterior wall; EDD, end-diastolic diameter.

prevalence of pleural effusion was significantly lower in DM-MI+Olmesartan than in DM-MI+Vehicle.

Infarct Size

Infarct size determined by the histomorphometric analysis of LV sections was comparable (61 ± 4% versus 59 ± 2%; P = NS) between DM-MI+Vehicle (n = 5) and DM-MI+Olmesartan (n = 5).

Histomorphometry

Myocyte cross-sectional area was significantly increased in DM-MI groups compared with control groups (Fig. 4).

TABLE 1. Blood Chemistry, Echocardiography, Hemodynamics, and Organ Weights

	Control+Vehicle	Control+Olmesartan	DM-MI+Vehicle	DM-MI+Olmesartan
Blood chemistry				
n	11	11	51	50
Blood glucose at 5 days, mg/dl	104 ± 5	109 ± 7	377 ± 9‡	380 ± 9‡
n	11	11	14	21
Blood glucose at 6 weeks, mg/dl	112 ± 5	120 ± 3	445 ± 28‡	473 ± 15‡
Echocardiography				
n	11	11	13	19
Heart rate, bpm	477 ± 9	475 ± 7	480 ± 7	483 ± 6
LVEDD, mm	4.0 ± 0.1	4.0 ± 0.1	6.0 ± 0.2‡	5.6 ± 0.1‡
LVESD, mm	2.6 ± 0.1	2.5 ± 0.1	5.3 ± 0.2‡	4.9 ± 0.1‡§
Ejection fraction, %	74.3 ± 0.9	75.7 ± 0.7	30.6±1.7 ‡	35.6 ± 1.3‡§
Hemodynamics				
n	11	11	12	12
Heart rate, bpm	453 ± 10	443 ± 13	467 ± 14	478 ± 8
Systolic blood pressure, mmHg	93 ± 2	93 ± 2	85 ± 2†	78 ± 2‡
$LVdP/dt_{max}$, mmHg/sec	10874 ± 684	11548 ± 601	4425 ± 431‡	5664 ± 389‡
$LVdP/dt_{min}$, mmHg/sec	8555 ± 537	8576 ± 314	2836 ± 230‡	3365 ± 194‡
LVEDP, mmHg	1.0 ± 0.5	1.2 ± 0.6	23.3 ± 1.7‡	13.0 ± 1.8‡¶
Organ weights				
n	11	11	14	21
Body wt, g	35.1 ± 0.9	35.3 ± 0.9	28.2 ± 1.1‡	29.2 ± 1.1‡
TL, mm	20.6 ± 0.8	20.3 ± 0.9	21.1 ± 0.1	21.2 ± 0.1
LV wt/TL, mg/mm	3.7 ± 0.3	3.6 ± 0.1	3.3 ± 0.1	3.1 ± 0.1*
Lung wt/TL, mg/mm	7.2 ± 0.3	7.7 ± 0.2	16.0 ± 1.4‡	12.3 ± 1.0‡§
Pleural effusion, %	—	—	86	48§

Values are means ± SEM.
†$P < 0.05$ vs. Control+Vehicle.
‡$P < 0.01$ vs. Control+Vehicle.
§$P < 0.05$ vs. DM-MI+Vehicle.
¶$P < 0.01$ vs. DM-MI+Vehicle.
LV, left ventricular; EDD, end-diastolic diameter; ESD, end-systolic diameter; EDP, end-diastolic pressure; wt, weight; TL, tibial length.

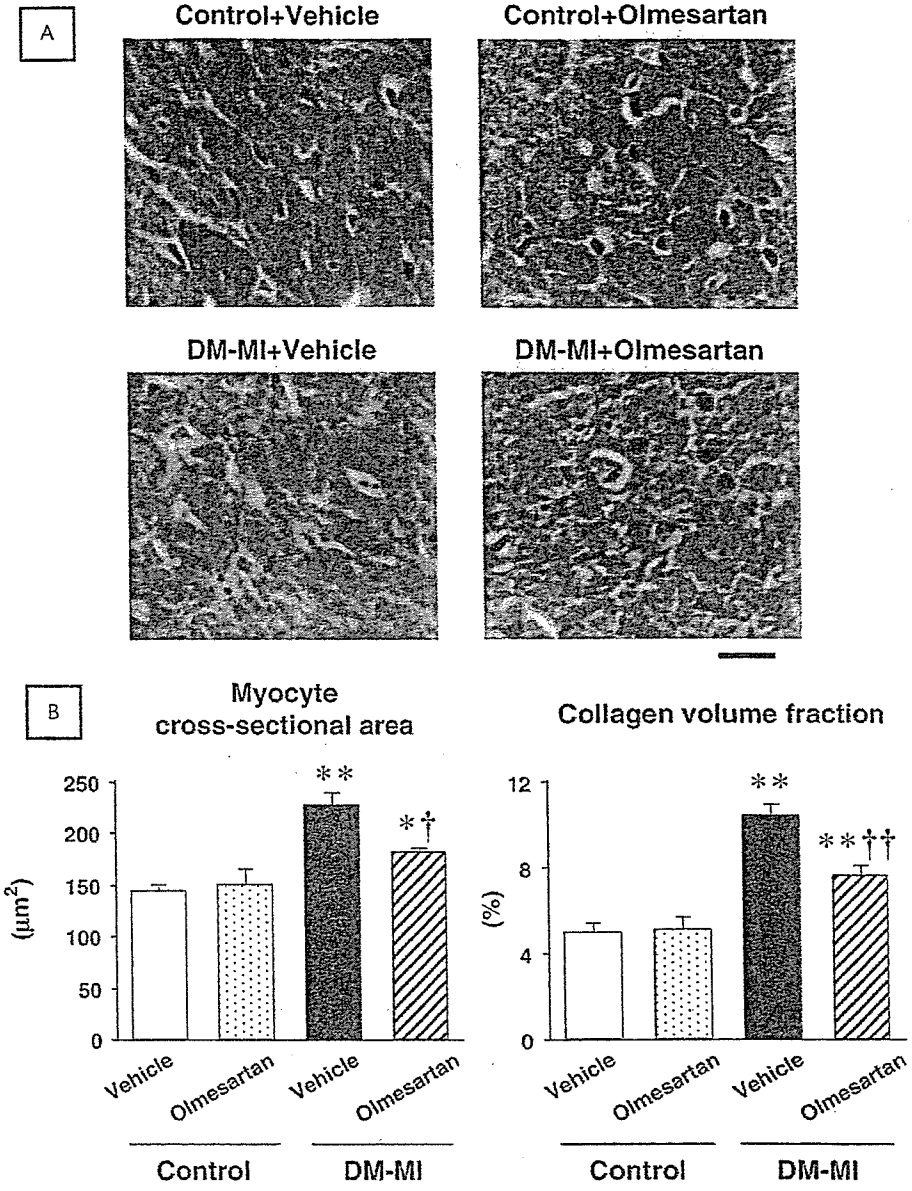

FIGURE 4. (A) Representative light microscopic photomicrographs of Masson's trichrome-stained myocardial sections obtained from Control+Vehicle, Control+Olmesartan, DM-MI+Vehicle, and DM-MI+Olmesartan mice. Scale bar represents 10 μm. (B) Summarized data for myocyte cross-sectional area and collagen volume fraction from Control+Vehicle, Control+Olmesartan, DM-MI+Vehicle, and DM-MI+Olmesartan (n = 5 for each) mice. Values are means ± SEM. *$P < 0.05$, **$P < 0.01$ for difference from the Control+Vehicle value. †$P < 0.05$, ††$P < 0.01$ for difference from the corresponding DM-MI+Vehicle value.

Collagen volume fraction was also increased in DM-MI groups. Both of this increase was significantly ameliorated in DM-MI+Olmesartan (Fig. 4).

Myocardial AT_1 receptor

AT_1 receptor gene expression was 1.9-fold increased in the LV from DM-MI mice compared to control mice ($P < 0.05$).

TGF-ß and MMPs/TIMPs

TGF-ß mRNA was significantly increased in DM-MI+Vehicle, and this increase was attenuated in DM-MI+Olmesartan (Fig. 5).

MMP-2 mRNA levels significantly increased in the DM-MI compared with control mice (Fig. 6). This increase was significantly attenuated in DM-MI+Olmesartan. Other MMPs, including MMP-1, -3, -8, and -9, were not altered in these mice (Fig. 6). The changes of TIMPs (TIMP-1, -2, -3, and -4) were also comparable between DM-MI+Vehicle and DM-MI+Olmesartan.

Apoptosis

There were rare TUNEL-positive nuclei in control mice. The number of TUNEL-positive cells in the noninfarcted LV was increased in the DM-MI groups. It decreased in DM-MI+Olmesartan compared with DM-MI+Vehicle (Fig. 7A). In addition, the intensity of DNA ladder indicated that the apoptosis in the noninfarcted LV from DM-MI+Olmesartan was attenuated compared with DM-MI+Vehicle (Fig. 7B).

DISCUSSION

In the presence of DM, MI mice had poor survival, decreased overall LV ejection performance, and exacerbated

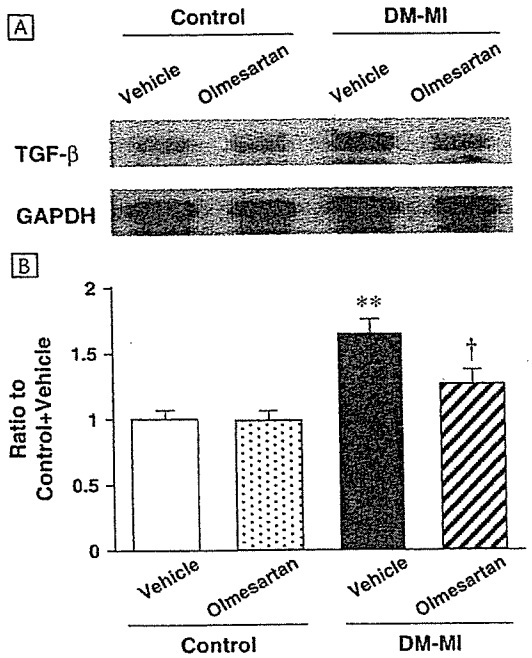

FIGURE 5. (A) Representative image of myocardial gene expression of TGF-β. (B) Densitometric analysis of TGF-β gene expression in Control+Vehicle (n = 6), Control+Olmesartan (n = 6), DM-MI+Vehicle (n = 8), and DM-MI+Olmesartan (n = 8) mice. Data were normalized by GAPDH concurrently run on the same gel and expressed as the ratio to Control+Vehicle values. Values are means ± SEM. $^{**}P < 0.01$ for difference from the Control+Vehicle value. $\dagger P < 0.05$ for difference from the corresponding DM-MI+Vehicle value.

LV remodeling, increased chamber dilatation as well as myocyte apoptosis and interstitial fibrosis of the noninfarcted myocardium, all of which were significantly ameliorated by the treatment of MI mice with olmesartan. Therefore, AngII may play a pivotal role in the development and exacerbation of heart failure after MI associated with diabetes.

Impact of DM in Post-MI LV Remodeling

MI leads to complex structural alterations (remodeling) involving both the infarcted and noninfarcted myocardium. Early remodeling is LV cavity dilatation occurring during the early phase of MI, which is likely due to wall thinning of the infarct region. During the first several days, LV enlargement follows; thereafter, a progressive dilatation of the noninfarcted LV associated with myocyte hypertrophy and interstitial fibrosis occurs over weeks. These progressive changes in LV geometry contribute to the development of depressed cardiac function, clinical heart failure, and increased mortality. Our recent study has demonstrated that hyperglycemia per se exacerbates post-MI LV remodeling and failure.[6] In diabetic MI mice, myocyte hypertrophy and apoptosis in association with interstitial fibrosis were more enhanced in diabetic post-MI hearts. These results indicate that post-MI remodeling processes might be mutually reinforcing in the setting of MI associated with DM, and DM may further enhance the development of heart failure. This may explain, at least in part, the clinical findings that the outcome after MI in diabetic patients is worse than that in nondiabetic patients.[1,2,5]

Effects of ARB on Post-MI Remodeling and Failure with DM

Accumulating evidence suggests that the cardiac renin-angiotensin system (RAS) is activated during the development and progression of LV remodeling and failure after MI[18] and that ACE inhibitors and ARBs have the favorable effects on these deleterious processes.[11,19] In addition, recent studies have shown that the RAS is activated also in DM.[20] Therefore, the combination of DM and MI together may synergistically activate the RAS in the heart, which may further damage its function and

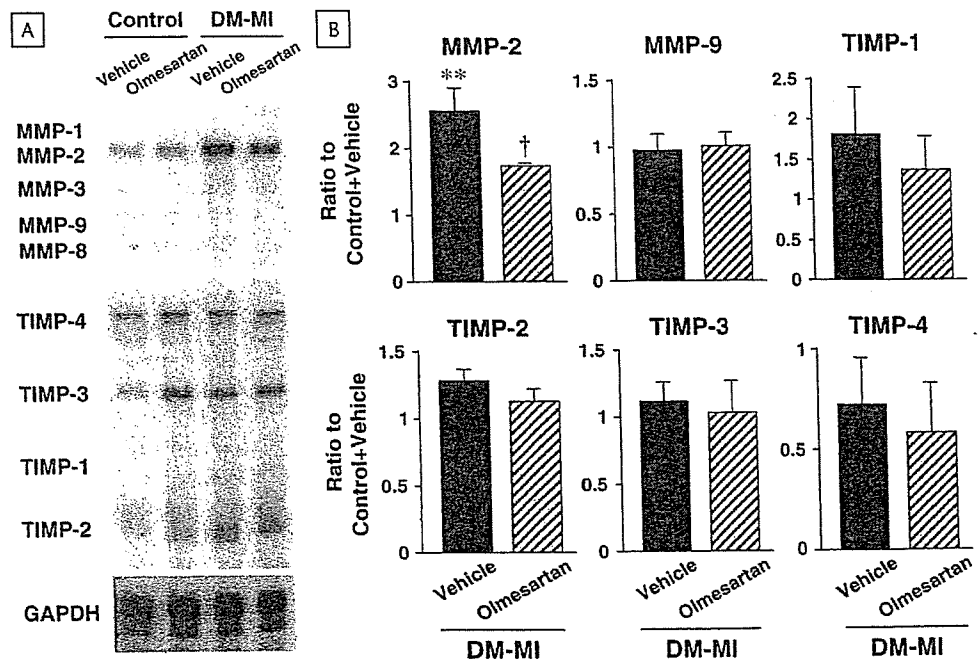

FIGURE 6. (A) Representative images of myocardial gene expression of MMPs/TIMPs. (B) Densitometric analysis of MMP and TIMP gene expression from DM-MI+Vehicle (n = 4) and DM-MI+Olmesartan (n = 4) mice. Each value was normalized to that of GAPDH in each template set as an internal control and expressed as the ratio to Control+Vehicle (n = 4). Values are means ± SEM. $^{**}P < 0.01$ for difference from the Control+Vehicle values. $\dagger P < 0.05$ for difference from the corresponding DM-MI+Vehicle values.

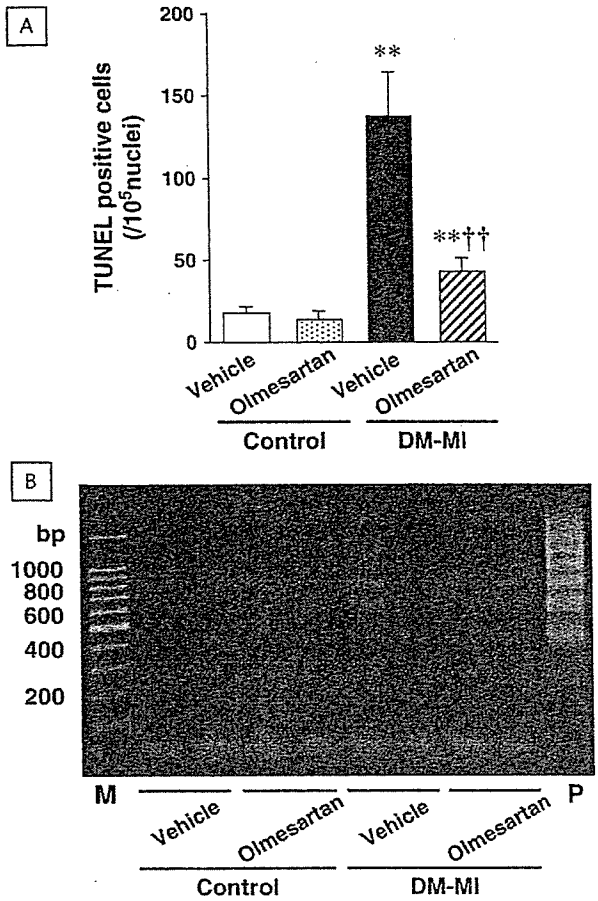

FIGURE 7. (A) The number of TUNEL-positive cells in the noninfarcted LV from Control+Vehicle, Control+Olmesartan, DM-MI+Vehicle, and DM-MI+Olmesartan (n = 5 for each) mice. Values are means ± SEM. $^{**}P < 0.01$ for difference from the Control+Vehicle values. $^{††}P < 0.01$ for difference from the corresponding DM-MI+Vehicle values. (B) DNA ladder indicative of apoptosis was detectable in the genomic DNA from the noninfarcted LV. M, 100 bp DNA ladder markers; P, positive control.

structure.[21] However, the beneficial effects of ACE inhibitors or ARBs in the context of diabetic MI have not been previously investigated. The present study clearly demonstrates that the post-MI LV remodeling and failure in DM were ameliorated by olmesartan, providing further evidence that AngII plays a pivotal role in the exacerbated heart failure after MI with diabetes.

Mechanisms of Beneficial Effects by ARB

There may be several factors attributable to the protective effects conferred by olmesartan on post-MI remodeling and failure. They were not due to its MI size-sparing effects because the infarct size was comparable between DM-MI+Vehicle and DM-MI+Olmesartan mice (Table 1). Further, its effects were not attributable to those on glycemic control. More importantly, they were independent of hemodynamics because blood pressure and heart rate were not altered (Table 1). Diabetes-induced acceleration of post-MI LV remodeling was associated with a significant increase in myocyte hypertrophy and interstitial fibrosis. The improved LV function by olmesartan was associated with a significant decrease in these hypertrophic and fibrotic changes in the noninfarcted LV (Fig. 4). One proposed mechanism by olmesartan for inhibiting LV structure alterations in DM-MI is related to a decrease in TGF-β expression and the resultant amelioration of cardiac fibrosis by olmesartan (Fig. 5). TGF-β is a locally generated cytokine that has been implicated as a major stimulator of tissue fibrosis. It has a major influence on fibroblast proliferation and extracellular matrix (ECM) production, particularly of collagen and fibronectin, while reducing degradation of these components. Because TGF-β is one of growth factors that influence tissue repair and remodeling, its activation might be well expected to play an important role in LV structural changes after MI. Olmesartan might directly ameliorate the increased expression of myocardial TGF-β expression in DM-MI mice because AngII is a well-known mediator to induce and activate TGF-β.[22] Another possible mechanism is the attenuation of myocardial MMP-2 expression in DM-MI+Olmesartan mice. It has been reported that myocardial MMPs are increased in MI.[23] Further, the inhibition of MMPs has been shown to limit the chamber remodeling after MI.[23] Therefore, MMP activation might play an important role in the pathophysiology of LV remodeling. Myocardial MMPs can be activated by AngII.[24] On the basis of these findings, the activation of myocardial RAS could contribute to the activation of myocardial MMP-2 and thus to the development of LV remodeling. Finally, recent studies have demonstrated that apoptosis is thought to contribute to the progressive deterioration of LV function after MI. Previous studies have demonstrated that apoptosis appears in not only infarcted but also noninfarcted myocardium after MI.[25] Specifically, apoptosis occurs in the noninfarcted LV late after MI. This is an intriguing observation in light of the remodeling process known to occur within the noninfarcted area, which is characterized by loss of myocytes, hypertrophy of remaining myocytes, and interstitial replacement fibrosis. In fact, recent studies have suggested that cardiac myocyte apoptosis contributes to LV remodeling after MI.[26,27] Moreover, AngII can mediate myocyte apoptosis, which may lead to myocardial remodeling and failure. Therefore, in DM-MI mice, olmesartan could directly ameliorate apoptosis and eventual post-MI cardiac failure.

Limitations

First, the present study could not elucidate the mechanism of death, arrhythmias or depressed cardiac function, because the telemetry of electrocardiograms was not performed. More importantly, it remains uncertain whether the beneficial effects of ARB could be attributable to the reduction of arrhythmic or heart failure death. Second, we used only olmesartan and did not examine the effects of other ARBs or ACE inhibitors in the present study. Therefore, we could not comment whether our findings are specific for olmesartan or other ARBs and ACE inhibitors could provide similar beneficial effects. Third, the changes in ECM synthesis/degradation diversely affect LV remodeling among different sites within the LV. However, we performed the biochemical analysis only in the noninfarcted LV from MI mice because the amount of tissue was very limited in the infarcted and border zone LV. Moreover, the molecular and biochemical alterations of ECM

especially at the noninfarcted LV are involved in the development and progression of post-MI remodeling and failure.

Clinical Implications

A number of clinical studies have reported that the prognosis after MI is worse in diabetic patients because they exhibit a higher incidence of heart failure and death compared with nondiabetic patients.[4] This may be due to the concomitant presence of severe coronary atherosclerotic lesions in diabetic patients. However, both experimental and clinical studies have shown that DM causes a specific form of myocardial damage independent of coronary atherosclerosis and manifests itself as LV dysfunction.[28] In addition to an acceleration of coronary atherosclerosis and an impairment of collateral formation, diabetes-induced exacerbation of LV remodeling and failure after MI is an important pathogenic mechanism responsible for this phenomenon.[6] The findings in the present study may further draw attention to the early and intensive treatment of heart failure by using ACE inhibitors or ARBs in diabetic patients with MI. Clinical evidence has further confirmed that these drugs improve the mortality and morbidity of patients with MI and heart failure.[7,8,29]

CONCLUSIONS

In the presence of diabetes, the cardiac RAS may mediate the acceleration of post-MI LV remodeling, and the inhibition of this system may reduce the diabetes-associated exacerbation of post-MI LV remodeling and failure.

ACKNOWLEDGMENTS

This study was supported in part by grants from the Ministry of Education, Science and Culture (No. 12670676, 14370230, 17390223, 17659223) and SANKYO CO., LTD. A part of this study was conducted in Kyushu University Station for Collaborative Research II.

REFERENCES

1. Haffner SM, Lehto S, Ronnemaa T, et al. Mortality from coronary heart disease in subjects with type 2 diabetes and in nondiabetic subjects with and without prior myocardial infarction. *N Engl J Med.* 1998;339:229–234.
2. Woodfield SL, Lundergan CF, Reiner JS, et al. Angiographic findings and outcome in diabetic patients treated with thrombolytic therapy for acute myocardial infarction: the GUSTO-I experience. *J Am Coll Cardiol.* 1996; 28:1661–1669.
3. Pfeffer MA, Braunwald E. Ventricular remodeling after myocardial infarction. Experimental observations and clinical implications. *Circulation.* 1990;81:1161–1172.
4. Stone PH, Muller JE, Hartwell T, et al. The effect of diabetes mellitus on prognosis and serial left ventricular function after acute myocardial infarction: contribution of both coronary disease and diastolic left ventricular dysfunction to the adverse prognosis. The MILIS Study Group. *J Am Coll Cardiol.* 1989;14:49–57.
5. Granger CB, Califf RM, Young S, et al. Outcome of patients with diabetes mellitus and acute myocardial infarction treated with thrombolytic agents. The Thrombolysis and Angioplasty in Myocardial Infarction (TAMI) Study Group. *J Am Coll Cardiol.* 1993;21:920–925.
6. Shiomi T, Tsutsui H, Ikeuchi M, et al. Streptozotocin-induced hyperglycemia exacerbates left ventricular remodeling and failure after experimental myocardial infarction. *J Am Coll Cardiol.* 2003;42:165–172.
7. Pfeffer MA, Braunwald E, Moye LA, et al. Effect of captopril on mortality and morbidity in patients with left ventricular dysfunction after myocardial infarction. Results of the survival and ventricular enlargement trial. The SAVE Investigators. *N Engl J Med.* 1992;327:669–677.
8. Dickstein K, Kjekshus J. Effects of losartan and captopril on mortality and morbidity in high-risk patients after acute myocardial infarction: the OPTIMAAL randomised trial. Optimal Trial in Myocardial Infarction with Angiotensin II Antagonist Losartan. *Lancet.* 2002;360:752–760.
9. Pfeffer MA, McMurray JJ, Velazquez EJ, et al. Valsartan, captopril, or both in myocardial infarction complicated by heart failure, left ventricular dysfunction, or both. *N Engl J Med.* 2003;349:1893–1906.
10. Schieffer B, Wirger A, Meybrunn M, et al. Comparative effects of chronic angiotensin-converting enzyme inhibition and angiotensin II type 1 receptor blockade on cardiac remodeling after myocardial infarction in the rat. *Circulation.* 1994;89:2273–2282.
11. Yoshiyama M, Takeuchi K, Omura T, et al. Effects of candesartan and cilazapril on rats with myocardial infarction assessed by echocardiography. *Hypertension.* 1999;33:961–968.
12. Mankad S, d'Amato TA, Reichek N, et al. Combined angiotensin II receptor antagonism and angiotensin-converting enzyme inhibition further attenuates postinfarction left ventricular remodeling. *Circulation.* 2001;103:2845–2850.
13. Cooper ME. Pathogenesis, prevention, and treatment of diabetic nephropathy. *Lancet.* 1998;352:213–219.
14. Effects of ramipril on cardiovascular and microvascular outcomes in people with diabetes mellitus: results of the HOPE study and MICRO-HOPE substudy. Heart Outcomes Prevention Evaluation Study Investigators. *Lancet.* 2000;355:253–259.
15. Shiomi T, Tsutsui H, Hayashidani S, et al. Pioglitazone, a peroxisome proliferator-activated receptor-gamma agonist, attenuates left ventricular remodeling and failure after experimental myocardial infarction. *Circulation.* 2002;106:3126–3132.
16. Usui M, Egashira K, Tomita H, et al. Important role of local angiotensin II activity mediated via type 1 receptor in the pathogenesis of cardiovascular inflammatory changes induced by chronic blockade of nitric oxide synthesis in rats. *Circulation.* 2000;101:305–310.
17. Matsusaka H, Ikeuchi M, Matsushima S, et al. Selective disruption of MMP-2 gene exacerbates myocardial inflammation and dysfunction in mice with cytokine-induced cardiomyopathy. *Am J Physiol Heart Circ Physiol.* 2005;289:H1858–1864.
18. Yamagishi H, Kim S, Nishikimi T, et al. Contribution of cardiac renin-angiotensin system to ventricular remodelling in myocardial-infarcted rats. *J Mol Cell Cardiol.* 1993;25:1369–1380.
19. Liu YH, Yang XP, Sharov VG, et al. Effects of angiotensin-converting enzyme inhibitors and angiotensin II type 1 receptor antagonists in rats with heart failure. Role of kinins and angiotensin II type 2 receptors. *J Clin Invest.* 1997;99:1926–1935.
20. Fiordaliso F, Li B, Latini R, et al. Myocyte death in streptozotocin-induced diabetes in rats in angiotensin II- dependent. *Lab Invest.* 2000;80:513–527.
21. Frustaci A, Kajstura J, Chimenti C, et al. Myocardial cell death in human diabetes. *Circ Res.* 2000;87:1123–1132.
22. Weber KT. Extracellular matrix remodeling in heart failure: a role for de novo angiotensin II generation. *Circulation.* 1997;96:4065–4082.
23. Hayashidani S, Tsutsui H, Ikeuchi M, et al. Targeted deletion of MMP-2 attenuates early LV rupture and late remodeling after experimental myocardial infarction. *Am J Physiol Heart Circ Physiol.* 2003;285:H1229–235.
24. Senzaki H, Paolocci N, Gluzband YA, et al. beta-blockade prevents sustained metalloproteinase activation and diastolic stiffening induced by angiotensin II combined with evolving cardiac dysfunction. *Circ Res.* 2000;86:807–815.
25. Palojoki E, Saraste A, Eriksson A, et al. Cardiomyocyte apoptosis and ventricular remodeling after myocardial infarction in rats. *Am J Physiol Heart Circ Physiol.* 2001;280:H2726–2731.
26. Sam F, Sawyer DB, Chang DL, et al. Progressive left ventricular remodeling and apoptosis late after myocardial infarction in mouse heart. *Am J Physiol Heart Circ Physiol.* 2000;279:H422–428.
27. Oskarsson HJ, Coppey L, Weiss RM, et al. Antioxidants attenuate myocyte apoptosis in the remote non-infarcted myocardium following large myocardial infarction. *Cardiovasc Res.* 2000;45:679–687.
28. Malhotra A, Reich D, Nakouzi A, et al. Experimental diabetes is associated with functional activation of protein kinase C epsilon and phosphorylation of troponin I in the heart, which are prevented by angiotensin II receptor blockade. *Circ Res.* 1997;81:1027–1033.
29. Pfeffer MA, McMurray J, Leizorovicz A, et al. Valsartan in acute myocardial infarction trial (VALIANT): rationale and design. *Am Heart J.* 2000;140:727–750.

Am J Physiol Heart Circ Physiol 292: H921–H927, 2007.
First published September 29, 2006; doi:10.1152/ajpheart.00019.2006.

Evaluation of transmural distribution of viable muscle by myocardial strain profile and dobutamine stress echocardiography

Takeshi Maruo,[1] Satoshi Nakatani,[1] Yintie Jin,[2] Kazunori Uemura,[2] Masaru Sugimachi,[2] Hatsue Ueda-Ishibashi,[3] Masafumi Kitakaze,[1] Tohru Ohe,[4] Kenji Sunagawa,[2] and Kunio Miyatake[1]

Departments of [1]Cardiology and [3]Pathology, National Cardiovascular Center, and [2]Department of Cardiovascular Dynamics, National Cardiovascular Center Research Institute, Osaka, Japan; and [4]Department of Cardiovascular Medicine, Okayama University Graduate School of Medicine, Okayama, Japan

Submitted 5 January 2006; accepted in final form 27 September 2006

Maruo T, Nakatani S, Jin Y, Uemura K, Sugimachi M, Ueda-Ishibashi H, Kitakaze M, Ohe T, Sunagawa K, Miyatake K. Evaluation of transmural distribution of viable muscle by myocardial strain profile and dobutamine stress echocardiography. *Am J Physiol Heart Circ Physiol* 292: H921–H927, 2007. First published September 29, 2006; doi:10.1152/ajpheart.00019.2006.—Transmural distribution of viable myocardium in the ischemic myocardium has not been quantified and fully elucidated. To address this issue, we evaluated transmural myocardial strain profile (TMSP) in dogs with myocardial infarction using a newly developed tissue strain imaging. TMSP was obtained from the posterior wall at the epicardial left ventricular short-axis view in 13 anesthetized open-chest dogs. After control measurements, the left circumflex coronary artery was occluded for 90 min to induce subendocardial infarction (SMI). Subsequently, latex microbeads (90 μm) were injected in the same artery to create transmural infarction (TMI). In each stage, measurements were done before and after dobutamine challenge (10 $\mu g \cdot kg^{-1} \cdot min^{-1}$ for 10 min) to estimate transmural myocardial viability. Strain in the subendocardium in the control stage increased by dobutamine (from 53.6 ± 17.1 to 73.3 ± 21.8%, $P < 0.001$), whereas that in SMI and TMI stages was almost zero at baseline and did not increase significantly by dobutamine [from 0.8 ± 8.8 to 1.3 ± 7.0%, P = not significant (NS) for SMI, from −3.9 ± 5.6 to −1.9 ± 6.0%, P = NS for TMI]. Strain in the subepicardium increased by dobutamine in the control stage (from 23.9 ± 6.1 to 26.3 ± 6.4%, $P < 0.05$) and in the SMI stage (from 12.4 ± 7.3 to 27.1 ± 8.8%, $P < 0.005$), whereas that in the TMI stage did not change (from −1.0 ± 7.8 to −0.7 ± 8.3%, P = NS). In SMI, the subendocardial contraction was lost, but the subepicardium showed a significant increase in contraction with dobutamine. However, in TMI, even the subepicardial increase was not seen. Assessment of transmural strain profile using tissue strain imaging was a new and useful method to estimate transmural distribution of the viable myocardium in myocardial infarction.

myocardial infarction; strain; viability; echocardiography

IT IS WELL KNOWN that myocardial contraction has transmural heterogeneity. Several experimental studies confirmed that the subendocardium contributes greater to overall myocardial thickening than the subepicardium (6, 25). On the other hand, when a reduction of coronary blood flow occurs, a severe reduction of perfusion and kinesis occurs in the subendocardium, but only a trivial reduction can be detected in the subepicardium (5, 31). After a long period of ischemia, myocardial necrosis progresses from the endocardium to the epicardium (8, 13).

Myocardial strain reflects regional myocardial function. With the recent advancement of tissue Doppler echocardiography, myocardial strain can be obtained noninvasively (3, 33) and has been reported to be useful to quantify regional myocardial systolic function in ischemic heart disease (9, 11, 24, 29, 36). The recently developed myocardial strain imaging system provides us myocardial strain in each wall layer and shows its distribution in a form of transmural myocardial strain profile (TMSP; see Ref. 1). Thus combination of TMSP and dobutamine stress echocardiography (DSE), which has been used for the assessment of myocardial viability (18), is expected to demonstrate transmural distribution of viability. There have been no methods to visualize distribution of myocardial viability over the ventricular wall in myocardial infarction, and such method would provide important information in the clinical situation.

In the present study, to assess the transmural extent of myocardial infarction, we investigated TMSP in subendocardial and transmural myocardial infarction dog models and quantified the transmural heterogeneity of myocardial viability using myocardial strain imaging with DSE.

MATERIALS AND METHODS

Experimental subjects and settings. We used 13 mongrel dogs (weighing 27.3 ± 2.2 kg). After induction with intravenous pentobarbital sodium (25 mg/kg body wt), they were anesthetized with 2% isoflurane with oxygen. A median sternotomy was performed, the pericardium was split from apex to base, and, after the instrumentation, the edges of the pericardial incision were loosely resutured. A 5-Fr. micromanometer-tipped catheter (model MPC-500; Millar Instruments, Houston, TX) was positioned in the left ventricle through the apex to obtain peak systolic left ventricular pressure and peak positive and negative dP/dt. Electrocardiogram (ECG) was monitored from limb leads. Left ventricular pressure signals and ECG were digitized online. The care and use of animals was in strict accordance with the guiding principles of the American Physiological Society, and the experimental protocol was approved by the National Cardiovascular Center Committees on Animal Experiments.

Experimental protocol. A 6-Fr. sheath was placed in the right femoral artery, and an angioplasty balloon catheter was positioned in the proximal segment of the left circumflex coronary artery by the standard catheterization technique. DSE (dobutamine infusion at 10 $\mu g \cdot kg^{-1} \cdot min^{-1}$ for 10 min) was used to assess myocardial viability. At the control stage, echocardiographic and hemodynamic measurements were done before and after DSE. A subendocardial myocardial infarction was created by inflating the balloon for 90 min

Address for reprint requests and other correspondence: S. Nakatani, Dept. of Cardiology, National Cardiovascular Center, 5-7-1, Fujishiro-dai, Suita, Osaka 565-8565, Japan (e-mail: nakatas@hsp.ncvc.go.jp).

The costs of publication of this article were defrayed in part by the payment of page charges. The article must therefore be hereby marked "*advertisement*" in accordance with 18 U.S.C. Section 1734 solely to indicate this fact.

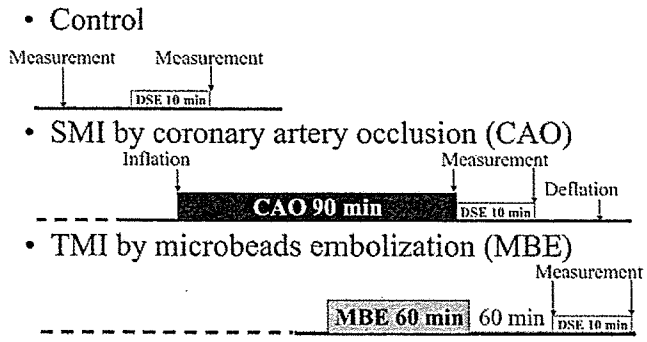

Fig. 1. Experimental protocol. DSE, dobutamine stress echocardiography; SMI, subendocardial myocardial infarction; TMI, transmural myocardial infarction.

(SMI stage; see Refs. 8 and 10), and DSE was performed during balloon inflation. After balloon deflation, 200–300 mg of latex microbeads (diameter 90 μm) were slowly injected in the same artery in 60 min to create a transmural myocardial infarction (TMI stage; see Refs. 7, 12, 15). At the TMI stage, DSE was performed 60 min after microbead embolization to complete myocardial infarction and to avoid ventricular instability to dobutamine challenge, and measurements were done before and after DSE (Fig. 1).

Ultrasound data acquisition. A commercially available ultrasound scanner (PowerVision 8000 3.5-MHz transducer; Toshiba, Tokyo, Japan) was used to obtain the epicardial left ventricular short-axis images at the level of basal and midventricle by tissue Doppler imaging. Recordings were stored in the form of digital loops of two cardiac cycles with 96–102 frames/s for subsequent analysis (33).

Tissue strain imaging. Strain is defined by the equation below and expresses the deformation of an object,

$$\text{Strain} = (L - L_0)/L_0$$

where L_0 is the length of an object before deformation and L is that after or during deformation. In echocardiography, L_0 is usually a muscle length at end diastole, and myocardial strain is used to express the deformation of local myocardial segments (4, 33).

In the present study, myocardial radial strain image was obtained from off-line analysis by using a research software TDI-Q (Toshiba; see Ref. 3). To obtain a strain image, TDI-Q software first calculates the myocardial displacement of all pixels of tissue by integrating myocardial velocity over a certain period. Because the frame rate was 96–102 frames/s, the step size for integration was 9.8–10.4 ms. Next, strain is obtained by evaluating the change of distance between pairs of two points defined on all pixels on the image by utilizing the displacement values. The distance of all two-pixel pairs at the initial time frame is equivalent to "L_0" on the above equation and set at 3 mm in this study (17). The initial time frame is set at end diastole to evaluate contraction; in other words "deformation" of the myocardium occurring in systole.

To measure local strain accurately, it is indispensable to obtain local velocity accurately. Therefore, the present myocardial strain imaging system has adopted tissue Doppler tracking and angle-correction techniques. Tissue Doppler tracking is an automatic motion tracking technique based on tissue Doppler information (30). By integrating a velocity of an indexed point on the ventricular wall known from tissue Doppler imaging, we can obtain myocardial displacement and predict the point where that point moves next. By repeating this procedure, the system can automatically track the motion of the point. With this technique, the influence of myocardial translation can be neglected. The angle-correction technique enables us to partly overcome the Doppler incident angle dependency that is inherent in Doppler echocardiography, as previous reports described (3, 26, 32). To correct the Doppler incident angle, a contraction center is set at the center of the left ventricular cavity at end systole in the left ventricular short-axis view. Next, the software automatically calculates the tissue velocity toward the contraction center (V_{motion}) by dividing the velocity toward a transducer (V_{beam}) by the cosine of the angle (θ) between the Doppler beam and the direction to the contraction center as follows:

$$V_{\text{motion}} = V_{\text{beam}}/\cos\theta$$

With the use of these two techniques, the research software TDI-Q automatically cancelled the effect of myocardial translation and angle dependency, accurately providing myocardial velocity, displacement, and strain (3). In the previously described experiments, the displacement data obtained by this method correlated with true displacement ($r = 0.99$, $P < 0.0001$; see Ref. 26).

Myocardial radial strain distribution over the myocardium is obtained as M-mode color-coded images, and the profile of distribution (TMSP) at end systole is shown as in Fig. 2. Bright color indicates high strain, and dark color indicates low strain. We obtained TMSP at basal and midinferolateral walls at end systole. We divided the myocardium into subendocardial and subepicardial half-layers by the midpoint of the myocardium at end systole. Mean strain values in the subendocardial half-layer and in the subepicardial half-layer were calculated by averaging strain values over each layer.

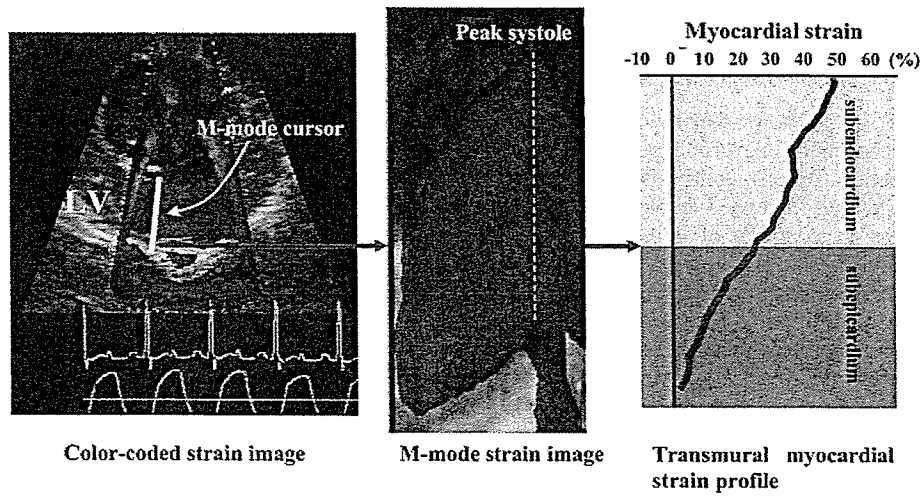

Fig. 2. Color-coded strain imaging, M-mode strain imaging, and transmural myocardial strain profile imaging in the control stage. *Left*: myocardial strain imaging of the left ventricular short axis at end systole. Red color means myocardial thickening. A white bar indicates an M-mode cursor. *Middle*: color-coded M-mode myocardial strain imaging obtained at the left ventricular posterior wall. The subendocardium is brighter than the subepicardium, indicating that the subendocardium contracts more vigorously. *Right*: transmural strain profile at end systole. The strain was highest at the subendocardium and lowest at the subepicardium, and the transmural strain showed a linear profile. LV, left ventricular wall.

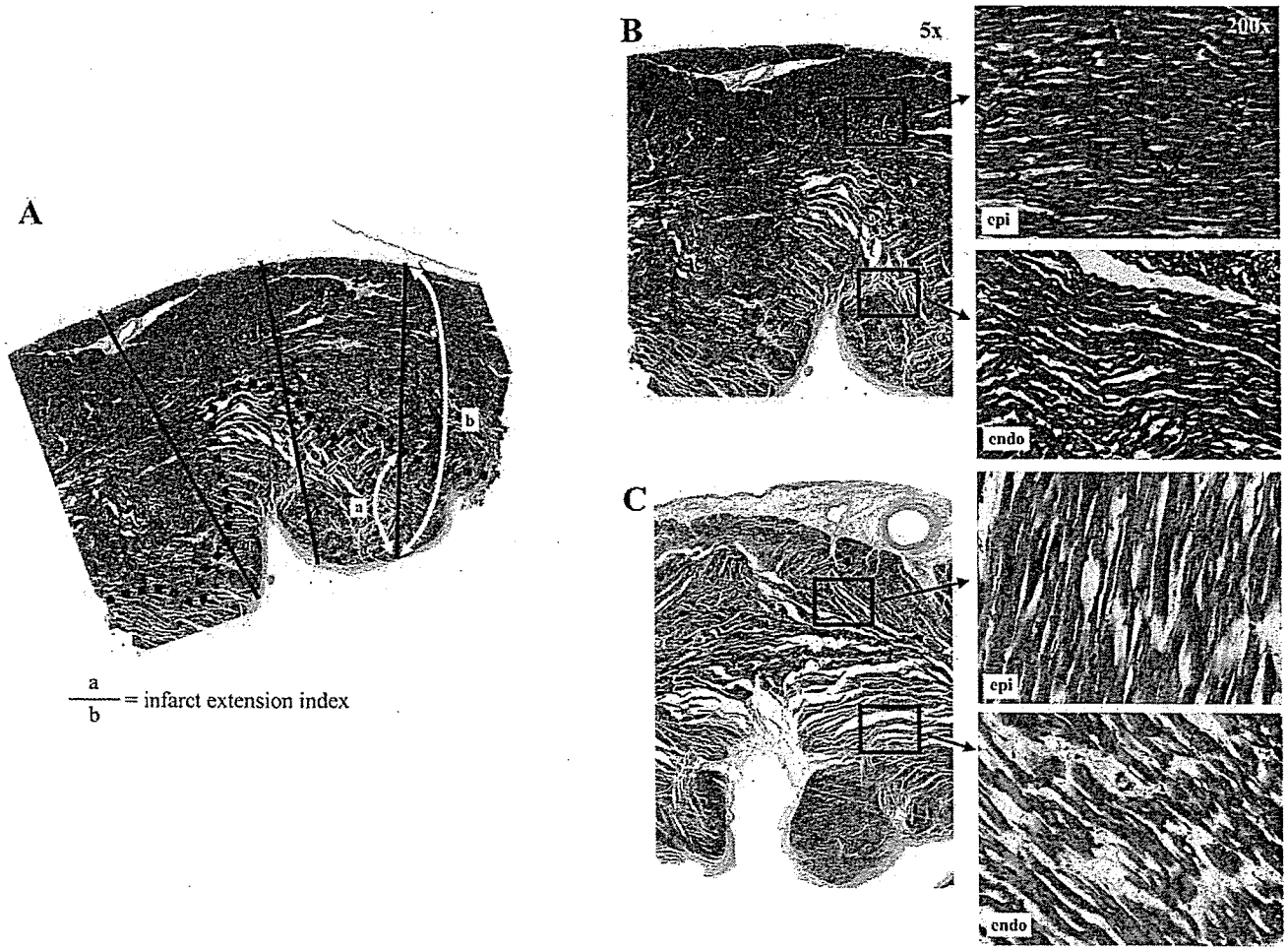

Fig. 3. *A*: determination of infarct extension index. Dotted line indicates the external limit of the infarcted zone. Examples of myocardial specimens taken after the SMI stage (*B*) and the TMI stage (*C*) stained by Masson's trichrome staining. In the SMI specimen, myocardial infarct was found only in the subendocardial layer, whereas acute ischemic changes such as wavy change or coagulation necrosis were recognized in both subendocardial and subepicardial layers in the TMI specimen. endo, Subendocardial layer; epi, subepicardial layer.

Histopathological studies. Establishment of subendocardial and transmural infarction by these techniques has been confirmed in our preliminary study and other previous studies (8, 10). We assessed the degree of extension of myocardial infarct also in the present study. At the end of the SMI stage in four dogs and the TMI stage in seven dogs, the heart was excised and cut into five to seven equally distant short-axis slices. Each slice was stained with hematoxylin-eosin and Masson's trichrome (Fig. 3). A pathologist who was blind to the experimental data examined the hearts histologically and measured the degree of infarct extension at the basal and midinferolateral walls, as previously reported (2). On each enlarged photomicrograph of the hearts, three to five transmural radii in the infarcted area were traced perpendicular to the endocardial and epicardial borders. The distance from the endocardial border to the external limit of the infarcted zone was measured and was expressed as a percentage of the distance between the endocardial and epicardial borders as an index of infarct extension, 100% being fully transmural and 0% being no infarction.

Table 1. *Hemodynamic parameters in control, SMI, and TMI stages*

	Baseline			DSE		
	Control (n = 13)	SMI (n = 11)	TMI (n = 7)	Control	SMI	TMI
HR, beats/min	133±17	128±27	129±27	149±22	134±27	150±19
LVP, mmHg	123±10*†	108±24	92±21	136±11†	132±28†	112±20
+dP/dt, mmHg/s	2,169±484*†‡	1,577±347*†	1,207±279*	4,021±979†‡	3,231±844†	2,478±1,138
−dP/dt, mmHg/s	−2,531±408*†	−1,824±606*†	−1,164±465*	−3,188±650†	−2,724±892	−2,104±526

Data are presented as means ± SD; n, no. of dogs. DSE, dobutamine stress echocardiography; SMI, subendocardial myocardial infarction; TMI, transmural myocardial infarction; HR, heart rate; LVP, peak systolic left ventricular pressure; +dP/dt, peak positive dP/dt; −dP/dt, peak negative dP/dt. $P < 0.05$ vs. DSE values (*), vs. SMI values (‡), and vs. TMI values (†).